Molecular Genetics and Metabolism Reports 21 (2019) 100524

Contents lists available at ScienceDirect

Molecular Genetics and Metabolism Reports

journal homepage: www.elsevier.com/locate/ymgmr

# Characterization of glycan substrates accumulating in GM1 Gangliosidosis

Roger Lawrence[a,*], Jeremy L. Van Vleet[a], Linley Mangini[a], Adam Harris[a], Nathan Martin[a], Wyatt Clark[a], Sanjay Chandriani[a], Jonathan H. LeBowitz[a], Roberto Giugliani[b], Alessandra d'Azzo[c], Gouri Yogalingam[a], Brett E. Crawford[a]

[a] Research, BioMarin Pharmaceutical Inc., Novato, CA 94949, USA
[b] Medical Genetics Service, HCPA, Department of Genetics, UFRGS, and INAGEMP, Porto Alegre, Brazil
[c] Department of Genetics, St. Jude Children's Research Hospital, Memphis, TN, USA

ARTICLE INFO

*Keywords:*
GM1 gangliosidosis
GLB1
Beta-galactosidase
Glycan metabolites
Disease biomarkers
Glycoanalysis

ABSTRACT

*Introduction:* GM1 gangliosidosis is a rare autosomal recessive genetic disorder caused by the disruption of the *GLB1* gene that encodes β-galactosidase, a lysosomal hydrolase that removes β-linked galactose from the non-reducing end of glycans. Deficiency of this catabolic enzyme leads to the lysosomal accumulation of GM1 and its asialo derivative GA1 in β-galactosidase deficient patients and animal models. In addition to GM1 and GA1, there are other glycoconjugates that contain β-linked galactose whose metabolites are substrates for β-galactosidase. For example, a number of N-linked glycan structures that have galactose at their non-reducing end have been shown to accumulate in GM1 gangliosidosis patient tissues and biological fluids.

*Objective:* In this study, we attempt to fully characterize the broad array of GLB1 substrates that require GLB1 for their lysosomal turnover.

*Results:* Using tandem mass spectrometry and glycan reductive isotope labeling with data-dependent mass spectrometry, we have confirmed the accumulation of glycolipids (GM1 and GA1) and N-linked glycans with terminal beta-linked galactose. We have also discovered a novel set of core 1 and 2 O-linked glycan metabolites, many of which are part of structurally-related isobaric series that accumulate in disease. In the brain of *GLB1* null mice, the levels of these glycan metabolites increased along with those of both GM1 and GA1 as a function of age. In addition to brain tissue, we found elevated levels of both N-linked and O-linked glycan metabolites in a number of peripheral tissues and in urine. Both brain and urine samples from human GM1 gangliosidosis patients exhibited large increases in steady state levels for the same glycan metabolites, demonstrating their correlation with this disease in humans as well.

*Conclusions:* Our studies illustrate that GLB1 deficiency is not purely a ganglioside accumulation disorder, but instead a broad oligosaccharidosis that include representatives of many β-linked galactose containing glycans and glycoconjugates including glycolipids, N-linked glycans, and various O-linked glycans. Accounting for all β-galactosidase substrates that accumulate when this enzyme is deficient increases our understanding of this severe disorder by identifying metabolites that may drive certain aspects of the disease and may also serve as informative disease biomarkers to fully evaluate the efficacy of future therapies.

## 1. Introduction

GM1 gangliosidosis is a Lysosomal Storage Disease (LSD) caused by defects in the *GLB1* gene which codes for β-galactosidase (EC 3.2.1.23), a lysosomal hydrolase that cleaves β-linked galactose residues from the non-reducing end (NRE) of glycan moieties found in various glycoconjugates. This rare autosomal recessive disease is characterized by the large lysosomal accumulation in the brain of GM1 ganglioside and its corresponding asialo derivative GA1, which are believed to cause severe neurodegeneration with profound effects on morbidity and

*Abbreviations:* A2G2, Oxford glycan naming designation for NA2 glycan; BMP, Bis(monoacylglycero) phosphate; dp, degree of polymerization; Gal, galactose; GLB1, β-galactosidase; GlcNAc, *N*-acetylglucosamine; GRIL-LC/MS, glycan reductive isotope labeling liquid chromatography mass spectrometry; Hex, hexose; HexNAc, *N*-acetylhexosamine; KS, keratan sulfate; Man, mannose; MPS, mucopolysaccharidosis; *m/z*, mass over charge; NRE, non-reducing end; TIC, total ion current; XIC, extracted ion current

* Corresponding author at: Research, BioMarin Pharmaceutical Inc., 105 digital Drive, Novato 94949, USA.
*E-mail address:* rlawrence@bmrn.com (R. Lawrence).

https://doi.org/10.1016/j.ymgmr.2019.100524
Received 19 July 2019; Received in revised form 10 September 2019; Accepted 13 September 2019
Available online 03 November 2019

mortality in most patients [1,2]. GM1 gangliosidosis is typically classified in three forms (infantile, juvenile, and adult) which have disease severities that are inversely proportional to residual enzyme activity. The early infantile onset form is the most devastating form, resulting in severe psychomotor retardation, hepatomegaly, splenomegaly and skeletal abnormalities [2].

There are two known lysosomal beta-galactosidases, GLB1 and galatosylceramidase (GALC), also known as galactocerebrosidase (EC 3.2.1.46). In the degradation of glycolipids, GALC appears to have a strong preference for β-linked galactose conjugated proximally to lipids such as in the case of galactosylceramide while GLB1 acts on β-linked galactose distal to the lipid moiety as seen in GM1 and GA1 gangliosides.

While commonly regarded as a gangliosidoses type LSD, β-galactosidase deficiency more accurately should be considered a broad spectrum oligosaccharidoses since, in addition to glycolipids, a substantial number of soluble N-linked glycans also accumulate in GM1 gangliosidosis. These disease-related oligosaccharides were detected in both affected tissues such as brain [3] and liver [4–6] as well as in biological fluids such as urine [7–18] and amniotic fluid [17,19]. The discovery of these additional storage metabolites is consistent with the role of β-galactosidase in removing β-linked galactose from the NRE of oligosaccharides moieties found not only in gangliosides but in other glycoconjugates such as glycoproteins and keratan sulfate proteoglycans (Fig. 1).

Morquio B syndrome is another LSD that arises from mutations in the *GLB1* gene resulting in defects in β-galactosidase activity that primarily effect the lysosomal degradation of keratan sulfate (KS) a glycosaminoglycan polysaccharide enriched in cartilage and cornea and made up of a repeat unit of galactose β-linked to *N*-acetylglucosamine-6-sulfate (Fig. 1). Unlike GM1 gangliosidosis patients, Morquio B patients exhibit mostly a skeletal phenotype with symptoms that are largely non-neuropathic [2,20]. However, cases with a phenotype merging GM1 gangliosidosis and Morquio B features have been described [21,22]. The reasons for the differences in clinical outcome and metabolite storage are not well understood but may stem from distinct subsets of *GLB1* mutations that preferentially impact different substrates. The observation that different mutations in *GLB1* result in distinct clinical outcomes and that β-galactosidase has numerous substrates argues for a deep profiling of substrates that accumulate as a result of β-galactosidase deficiency.

In this study we carried out a comprehensive survey of galactoside metabolite substrates of GLB1 that accumulate in a mouse model and in human GM1 gangliosidosis patients. We performed substrate analysis using glycan reductive isotope labeling liquid chromatography/mass spectrometry (GRIL LC/MS) [23,24] with data-dependent tandem mass spectrometry in order to detect a wide range of GLB1 substrate metabolites that accumulate in the absence of enzyme activity. We analyzed samples for glycolipids, gangliosides, N-linked and O-linked glycan metabolites. A number of unique soluble glycan metabolites, many of which are part of isobaric series composed of the same number of hexose (Hex) and *N*-acetylhexosamine (HexNAc) residues were detected in affected tissues. While a number of these soluble oligosaccharides have been previously described and determined to be predominantly N-linked glycan metabolites, we also detected a number of abundant O-linked pentasaccharide (dp5) species consistent with mucin-type O-linked glycans which have not been previously described. These O-linked metabolites were detected in multiple tissues and urine in GLB1 deficient mice as well as humans. None of these soluble glycan metabolites were detected in either human or murine unaffected control samples suggesting that they could make clinically relevant disease-specific biomarkers that can be conveniently measured in urine samples.

In addition to discovering new potential biomarkers, a better understanding of all of the β-galactosidase substrates that accumulate as a result of enzyme deficiency and their associated pathological impacts will broaden our understanding of the molecular and cellular mechanisms effected in this disease and may aid in evaluating efficacy of future therapeutics.

## 2. Materials and methods

### 2.1. Materials

The A2G2 (NA2) N-glycan, $^{13}C_6$-aniline, and sodium cyanoborohydride ($NaBH_3CN$), were purchased from (Sigma Aldrich, Milwaukee, WI, USA). The endoglycosidase Endo S was purchased from New England Biolabs (Ipswich, MA, USA). Hypersep Hypercarb PGC SPE cartridges (25 mg, 1 mL) and Pierce BCA Protein Assay Kit were purchased from ThermoFisher Scientific, Waltham, MA, USA). The Sep-PAK C18 solid phase extraction (SPE) cartridges (100 mg, 1 mL) was from Waters (Milford, MA, USA). All other chemicals were of reagent grade or LC/MS grade for chromatography systems. Human recombinant β-Galactosidase was prepared as described [25].

### 2.2. Human brain and urine samples

All human brain tissues were obtained from the NIH NeuroBioBank. The GM1 gangliosidosis sample was obtained from a female subject who passed away at the age of 9.96 years. Her initial diagnosis by post-mortem examination was inconclusive, but whole exome sequencing identified two mutations in *GLB1*, c.765G > C (p.Gln255His) and c.335A > C (p.His12Pro). Both mutations have previously been reported in GM1 gangliosidosis patients, and the observed genotype would be expected to lead to an age of death consistent with that observed.

Human urine samples from subjects diagnosed with GM1 gangliosidosis were obtained from the Hospital de Clinicas de Porto Alegre, Porto Alegre, Brazil.

All patient samples were collected and used for this study according to a protocol approved by the Institutional Review Board (IRB) of each submitting institution.

### 2.3. Gangliosides and BMP sample preparation

Brain samples were homogenized in water with 1.4 mm ceramic beads using an Omni Bead Ruptor 24 Homogenizer (Omni International, Kennesaw, GA, USA). Protein concentration of the homogenate was determined using BCA assay. All homogenates were diluted with water to 4 μg protein/μL homogenate. An amount of sample equal to 200 μg of protein was extracted with 95/5 methanol/glacial acetic acid (*v*/v). Samples were filtered through 10 kDa centrifugal filter tubes and stored at −20 °C until use.

### 2.4. Glycolipidomics and glycosphingolipid acyl group characterization

LC/MS analysis was performed on an Acquity UPLC system equipped with a HSS C18 column (1.8 μm, 1 mm × 150 mm) (Waters, Milford, MA, USA) connected to a Thermo LTQ Orbitrap XL mass spectrometer. Solvent A was 74% methanol, 25% water, 1% formic acid with 5 mM ammonium formate and solvent B was 99% methanol, 1% formic acid with 5 mM ammonium formate. The initial composition was 80% A/20% B at a flow rate of 0.1 mL/min with the column temperature kept at 50 °C. Samples equal to 35 μg of protein were eluted using a gradient method of 80% A/20% B isocratic for one minute, 80% A/20% B to 0% A/100% B from 1 min to 40 min, 0% A/100% B isocratic to 55 min, then re-equilibration at 80% A/20% B isocratic to 60 min.

The LTQ Orbitrap XL was operated in the negative ion mode and the sample introduced by ESI. The capillary temperature was set at 250 °C with a spray voltage of 3 kV and capillary voltage of −4 V. The sheath gas flow was set to 24 and the auxiliary gas flow to 3. Full scans were performed at a resolution of 60,000 and a range of 300–2000 *m/z*. Data-

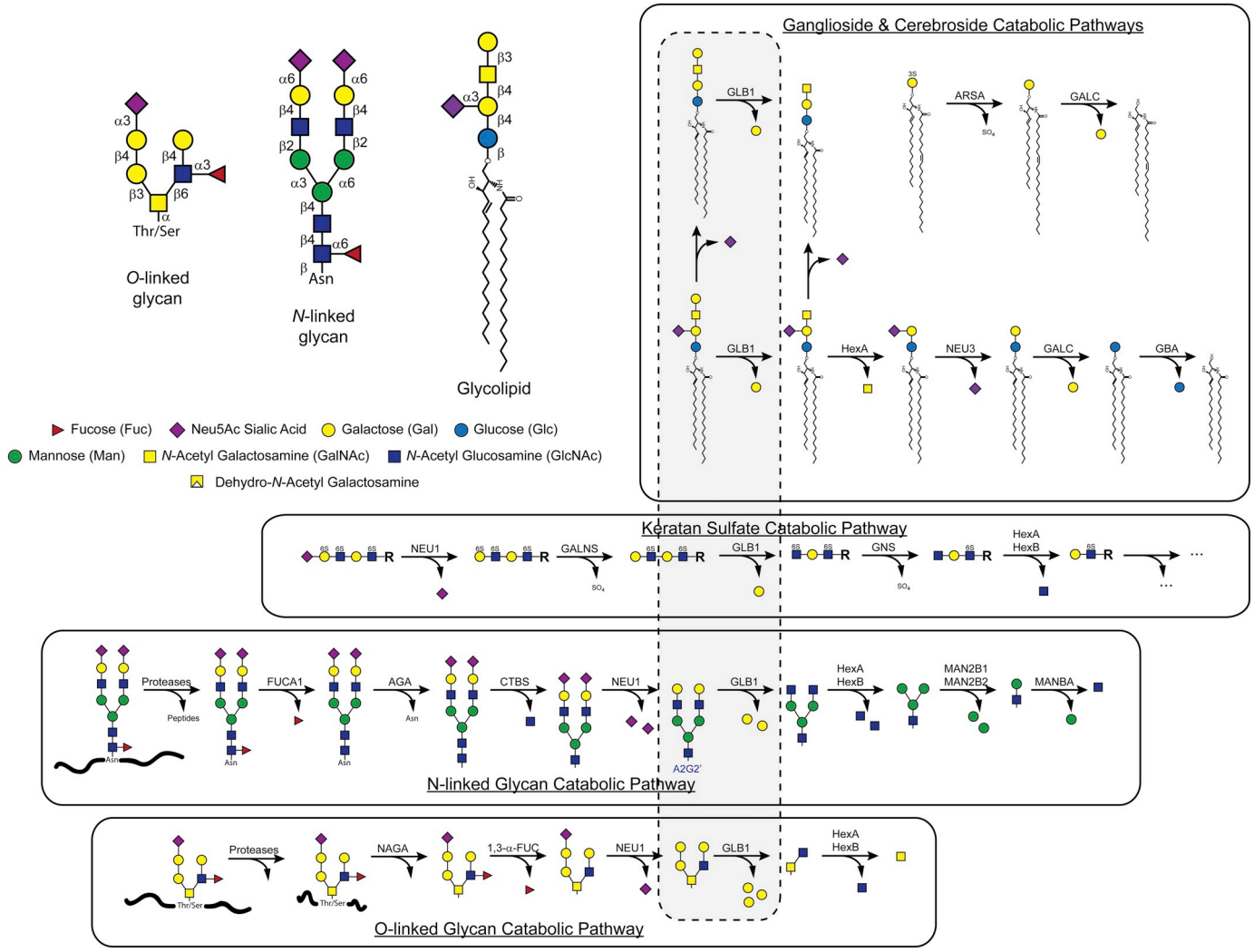


**Fig. 1.** Catabolic pathways for glycolipid and glycoproteins effected by β-galactosidase. The substrate target for β-galactosidase is β-linked galactose residues situated at the non-reducing end (NRE) of oligosaccharides found in many different glycoconjugates including glycolipids, glycosaminoglycans, and glycoproteins. Four common types of glycoconjugate oligosaccharides containing galactose are shown with their branching structures along with a glycan symbol map used in this paper (upper left). The catabolic pathways for GM1, Keratan Sulfate, N-linked glycans and O-linked glycans are shown (in boxes) along with the intermediate metabolite structures (shown in the grey field enclosed by the dashed line) having β-linked galactose at the NRE which are likely substrates for β-galactosidase and thus putative storage products that accumulate in β-galactosidase deficiency. For completeness, the catabolic pathway for sulfatides and galactosyl ceramide is included. The N-glycan metabolite formed in the N-glycan catabolic pathway A2G2' is also shown (blue font). Throughout this paper we use the Oxford notation scheme to refer to N-glycans and related metabolites such as A2G2 and A2G2'.

dependent collision induced dissociation (CID) was performed on the three most intense ions within the full scan using a normalized collision energy of 35 V and an activation time of 30 ms. The CID profile was used to detect glycolipids and specific acyl groups present in glycosphingolipids.

### 2.5. Ganglioside and BMP analysis

Samples were analyzed for five different gangliosides (GM1, GM2, GM3, GA1, GA2) and BMP (BMP 22:6) content with an Acquity UPLC attached to a Xevo TQ-S micro Triple Quadrupole Mass Spectrometer (Waters Corporation, Milford, MA).

For gangliosides, compounds were separated on an Acquity UPLC Glycan BEH Amide column (Waters Corporation, Milford, MA). Solvent A was 5 mM ammonium acetate in 94.5% acetonitrile, 2.5% methanol, 2.5% water, and 0.5% formic acid. Solvent B was water. The initial solvent composition was 95% A/ 5% B at a flow rate of 0.4 mL/min. The column was kept at 50 °C. The LC elution gradient profile was hold 95% A/ 5% B for 2 min, ramp to 50% A/ 50% B over 10 min, hold at 50% A/ 50% B for 10 min, then back to 95% A/5% B and hold for 4 min. Samples were ionized by ESI in positive ion mode. The capillary voltage was set at 1.0 kV, the desolvation temperature was set at 500 °C, and the desolvation gas flow was 1000 L/h. Two precursor-product ion transitions, one for the (d18:1/18:0) species, one for the (d18:1/20:0) species, were monitored for each of the five gangliosides as follows: GM1–1546.7 > 366.1, 1574.7 > 366.1; GA1–1255.7 > 366.1, 1283.8 > 366.1; GM2–1384.7 > 204.1, 1412.7 > 204.1; GA2–1093.6 > 264.3, 1121.6 > 292.3; GM3–1181.5 > 264.3, 1209.6 > 292.3. The sum of the two transitions for each ganglioside was used for quantitation. A standard reference curve containing all 5 gangliosides from 100 to 6.25 pg/μL was prepared with standards from Enzo Life Sciences, Inc. (Farmingdale, NY) in 95/5 methanol/glacial acetic acid (v/v).

For BMP phospholipid, compounds were separated with an Acquity UPLC HSS C18 column (Waters Corporation, Milford, MA). Solvent A was 5 mM ammonium formate in 74% methanol, 25% water, and 1% formic acid. Solvent B was 5 mM ammonium formate in 99% methanol, and 1% formic acid. The initial solvent composition was 80% A/ 20% B

at a flow rate of 0.1 mL/min. The column was kept at 50 °C. The LC elution gradient profile was hold 80% A/ 20% B for 1 min, ramp to 0% A / 100% B over 5 min, hold at 0% A/ 100% B for 10 min, then back to 80% A/ 20% B and hold for 4 min. Samples were ionized by ESI in negative mode. The capillary voltage was set at 3.5 kV, the desolvation temperature was set at 600 °C, and the desolvation gas flow was 1000 L/h. Two precursor-product ion transitions were monitored, 865.5 > 327.3 for BMP(22:6), and 665.4 > 227.2 for BMP(14:0). A standard reference curve containing BMP(14:0) from 100 to 6.25 pg/μL was prepared with a standard from Avanti Polar Lipids, Inc. (Alabaster, AL). Because BMP(22:6) was not commercially available, BMP(22:6) concentrations are reported as equivalents of BMP(14:0).

### 2.6. Biological sample preparation and glycan labeling

Tissues were homogenized, in water, with 1.4 mm ceramic beads using an Omni Bead Ruptor 24 Homogenizer (Omni International, Kennesaw, GA, USA) and debris was removed by centrifugation at 14,000 rpm and 8 °C for 20 min. The protein concentration of clarified extracts was determined by BCA assay. An amount of sample equivalent to 240 μg of protein, for tissues, or 100 μL, for urine, were diluted to 1 mL with water and subjected to SPE purification using a Hypersep Hypercarb PGE SPE cartridge following the manufacturer's instructions and dried by centrifugal evaporation. The purified free glycans were labeled with aniline by reductive amination as previously described [23,24] (15 μL aniline, 15 μL 1 M $NaCNBH_3$ in 70:30 DMSO:HOAc) at 37 °C for 18–24 h. After labeling the remaining aniline was removed by centrifugal evaporation at 37 °C. Samples were dissolved in water prior to analysis.

### 2.7. Internal standard preparation

In order to generate the A2G2' octasaccharide (dp8) standard, it was necessary to first cleave off the reducing end GlCNAc residue from the fully intact A2G2 (NA2) enneasaccharide (dp9). The A2G2 glycan (2000 pmoles) was digested with Endo S (800 units) in a total volume of 20 μL of 50 mM Sodium Phosphate pH 7.5 for 18–24 h followed by purification on a Sep-PAK C18 SPE cartridge (100 mg, 1 mL), as to the manufacturer's instructions, and dried by centrifugal evaporation. The dried resulting A2G2' glycan standard was then labeled with $^{13}C_6$-aniline (15 μL, 15 μL 1 M NaCNBH3 in 70:30 DMSO:HOAc) at 37 °C for 18–24 h and the remaining $^{13}C_6$-aniline was removed by centrifugal evaporation. Prior to analysis, the internal standard was dissolved in water.

### 2.8. LC/MS analysis and quantitation of A2G2'

LC/MS analysis was performed on an Acquity UPLC system equipped with a Glycan BEH Amide HILIC column (1.7 μm, 2.1 mm × 150 mm) (Waters, Milford, MA, USA) connected to a Thermo LTQ Orbitrap XL mass spectrometer. Solvent A was 100 mM Ammonium Formate pH 4.5 and Solvent B was Acetonitrile with an initial composition of 22% A/78% B and a flow rate of 0.2 mL/min. The column temperature was kept at 60 °C. Prior to injection an amount of aniline labeled sample equal to 70 μg of protein, for tissues, or 20 μL, for urine, was placed in a LC-MS sample vial along with 10 pmoles of $^{13}C_6$-aniline labeled A2G2' biomarker internal standard and dried by centrifugal evaporation. The samples were then dissolved in a solution of 22% A/78% B. The labeled free glycans were eluted using a gradient profile of 22% A/78% B to 37% A/63% B over 65 min, 100% A/0% B for 6 min, 100% A/0% B to 22% A/78% B in 5 min and held there for 9 min.

The LTQ Orbitrap XL was operated in the positive ion mode and the sample introduced by ESI. The capillary temperature was set at 250 °C with a spray voltage of 2 kV. The sheath gas flow was set to 58 and the auxiliary gas flow to 9. Full scans were performed at a resolution of 60,000 and a range of 200–2250 *m/z*. Data-dependent collision induced dissociation (CID) was performed on the three most intense ions in the full scan using a normalized collision energy of 35 V and an activation time of 30 ms. The N-glycan A2G2' metabolite was determined by ratiometric comparison of the $[^{12}C_6]$aniline labeled endogenous A2G2' ion abundance with that of the known molar amount of the internal standard spike as previously described [23].

### 2.9. GRIL-LC/MS analysis of urinary keratan sulfate levels

Urinary glycosaminoglycan (GAG) polysaccharides were purified as previously described for GAG isolations [23]. Briefly, GAG chains in 50 μL of urine were extracted by digestion with Pronase (Sigma-Aldrich) at 37 °C for 24 h followed by anion-exchange chromatography (DEAE-Sephacel, GE Healthcare Life Sciences, Marlborough, MA) and subsequent desalting by size-exclusion chromatography (PD10 columns, GE Healthcare Life Sciences, Marlborough, MA). After extraction, urinary KS polysaccharide chains were subjected to enzymatic depolymerization with keratinase II (Glycosyn Technologies, Lower Hutt, New Zealand) which cleaves glycosidic linkages between GlcNAc6S and either galactose or galactose 6-sulfate releasing both disaccharide and larger oligosaccharide residues that can be subsequently analyzed by GRIL-LC/MS [23]. Each sample was reconstituted in 50 μL 10 mM sodium acetate and digested with 4 mU of keratinase II for 16 h at 37 °C before labeling with aniline as previously described [23]. While all of the urinary KS samples were labeled with $[^{12}C_6]$aniline after depolymerization, an additional aliquot from one of the normal urine samples (NHU4499) was also labeled with $[^{13}C_6]$aniline for use as a differentially isotope-labeled internal reference standard. Equal amounts of this internal reference standard were added to all of the $[^{12}C_6]$aniline labeled samples and analyzed by GRIL-LC/MS. Ion abundances for the principal products from keratanase II digestion: g0A6, g6A6, g0A6g0A6, and g0A6g6A6 (nomenclature previously described [26]) as well as the fucosylated products g0A6(f0), g0A6g0A6(f0), g0A6(f0) g0A6(f0), g6A6g6A6(f0), and Neu5Ac-g0A6g0A6(f0) were summed together to give an aggregate ion intensity. The relative difference in total urinary KS levels was determined ratiometrically by comparison to the heavy isotope-labeled reference standard after normalization to creatinine. For example, each sample's aggregate digestion product ion intensity was divided by the corresponding aggregate digestion product ion intensity for the reference standard. This ratio was then multiplied by the ratio of creatinine levels in the sample and the internal reference standard giving the relative difference in KS levels between the two.

### 2.10. Quantitative analysis of galactose from free glycans by high pH anion exchange chromatography with pulsed amperometric detection (HPAEC-PAD)

Free glycans from mouse brain samples (210 μg protein equivalent) were dissolved in 20 μL of 50 mM Sodium Acetate Buffer pH 4.5 and incubated overnight with β-Galactosidase (4 mU) at 37 °C to release terminal galactose residues. Enzyme was removed from the samples using a Sep-PAK C18 SPE cartridge (100 mg, 1 mL) as described above, and the resulting flow thru and washes were brought to dryness by centrifugal evaporation. Released galactose was analyzed by HPAEC-PAD using a Dionex ICS-5000+ Ion Chromatography system equipped with a pulsed amperometric detector (Thermo Fisher Scientific, Waltham, MA, USA). Separation was performed using a CarboPac PA20 IC column (3 × 150 mm, Thermo) and guard (3 × 30 mm, Thermo) at a column temperature of 30 °C and a flow rate of 0.5 mL/min with an injection volume of 100 μL. Monosaccharides in each sample (equivalent to 80 μg protein) were separated isocratically in 12.5 min with 10 mM NaOH. Analytes were detected with a gold electrode, using the following electric potentials: $E_1 = +0.1$ V for 0.4 s (integrating from 0.2 s to 0.4 s), $E_2 = -2.0$ V (0.02 s), $E_3 = +0.6$ V (0.01 s), and $E_4 = -0.1$ V (0.06 s). The amount of galactose detected in each sample

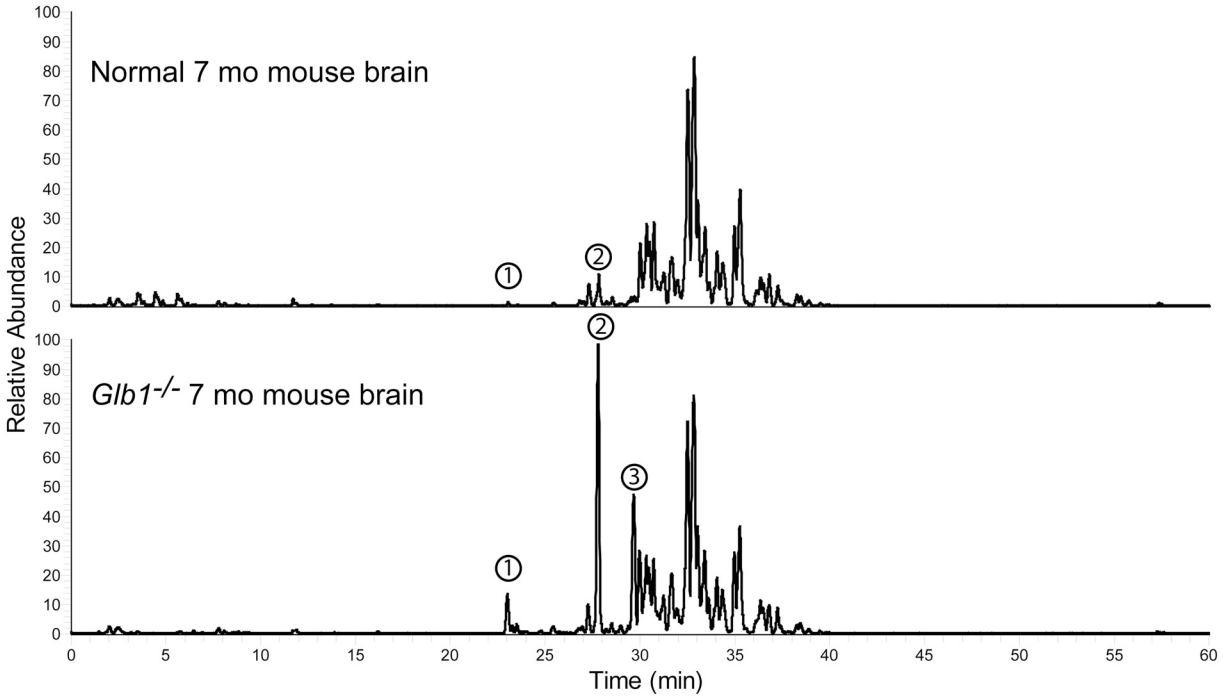


**Fig. 2.** LC/MS lipidomics screen of mouse brain homogenates for accumulating lipids and glycolipids in *GLB1* null mouse brain. The lipidomics profile of acidic methanol extracts made from water homogenates of whole brain from a 7-month-old normal mouse (top trace) and a 7-month-old *Glb1*$^{-/-}$ mouse (bottom trace) were compared. The total ion current chromatograms (negative ion mode) for both samples are shown normalized to the same scale (relative abundance). Three peaks numbered 1–3 corresponding to Bis(monoacylglycero) phosphate (22:6) (BMP(22:6), peak 1), GM1(d18:1/18:0) (peak 2), and GA1(d18:1/18:0) (peak 3) were observed to be elevated in the *GLB1* null sample compared to the normal control.

was calculated by comparing the sample galactose peak area to the peak area of a known amount of galactose standard using Chromeleon 7.2 Chromatography Data System Software (Thermo) and normalized to amount of protein.

## 3. Results

### 3.1. Liquid chromatography/mass spectrometry analysis of brain homogenates from GLB1 null mice showed the disease-related accumulation of ganglioside and phospholipid

As part of our comprehensive screen to identify unrecognized β-galactosidase substrates that accumulate in GM1 gangliosidosis, we performed lipidomics analysis on samples made by extracting brain homogenates with acidic methanol to recover polar lipids including glycolipids. We analyzed brain extracts from a 7-month-old normal mouse and a 7-month-old *GLB1*$^{-/-}$ mouse [27] by performing reverse phase LC/MS in the negative ion mode. Predominating ions were subjected to data-dependent MS/MS product ion analysis using collision induced dissociation (CID). We detected three peaks (number 1–3 in Fig. 2) having significantly higher abundance in the *GLB1* null mouse compared to the age-matched normal control. Little or no signal was detected for peak 3 in the normal control and thus it showed the greatest fold increase. The *m/z* values and CID profile for these three species correspond to Bis(monoacylglycero) phosphate (22:6) (BMP (22:6)), GM1(d18:1/18:0), and GA1(d18:1/18:0), respectively. No other accumulating lipid species extractable under the conditions used were detected in the knockout mouse brain sample suggesting that these are the only lipids showing large increases due to β-galactosidase deficiency. The rest of the peaks detected in both *GLB1* null and normal mice have *m/z* values consistent with various phospholipids and only BMP(22:6) exhibited significant accumulation in the knockout mouse (Fig. 2). This phospholipid species is a negatively charged glycerophospholipid enriched in endosomal/lysosomal membranes and known to be a biomarker for phospholipidosis [28,29] and a storage lipid that accumulates in GM1 gangliosidosis [30] thus, like GM1/GA1, its elevation was expected. We did not detect increases in the steady state levels for non-ganglioside glycolipids including lactosylceramide, galactosyl ceramide, sulfatides, and monogalactosyldiacylglycerol resulting from the disruption of the *GLB1* gene. Thus, other than the expected glyco- and phospho-lipids, we found no alternative lipid containing disease-related biomarkers.

In order to further characterize the gangliosides accumulating in the *GLB1* null mouse brain, we determined the most abundant acyl-isoforms of GM1. We examined the product ion profile generated for the most abundant ions during data-dependent collision induced dissociation (CID). Using this method, sialo glycolipids can be identified by the neutral loss of 291 Da corresponding to Neu5Ac sialic acid. This approach revealed 12 different glycosphingolipids including lyso-GM1, GM1 containing one of 8 different acyl groups, GM2, GM3 and GD1 (Supplemental Fig. 1). Most of these were obscured by the more abundant phospholipids seen in Fig. 2 but were resolved by the data-dependent CID. The steric acid containing GM1 ganglioside, GM1(d18:1/18:0), was by far the most abundant isoform followed by GM1(d18:1/20:0) together accounting for 93.8% (86.6% and 7.2%, respectively) of the ion abundance attributable to GM1. Consequently, these two species were chosen as the sole GM1 species to monitor using LC/MS/MS for quantitative analysis. Furthermore, since GA1 is a product of GM1 accumulation and both GM2 and GM3 are common intermediates to GM1 in the biosynthetic pathway, GA1, GM2, GA2, and GM3 containing these two acyl chains were chosen as isoforms to monitor for ganglioside profiling of brain samples.

We evaluated the ion abundance for all sialo ganglioside species in the normal control sample and detected only GM1(d18:1/18:0) with a smaller amount of GM1(d18:1/18:1) and GM2(d18:1/18:0) (data not shown).

We developed a quantitative LC/MS/MS assay to analyze GM1/GA1, GM2/GA2 and GM3 gangliosides with the two most abundant acyl

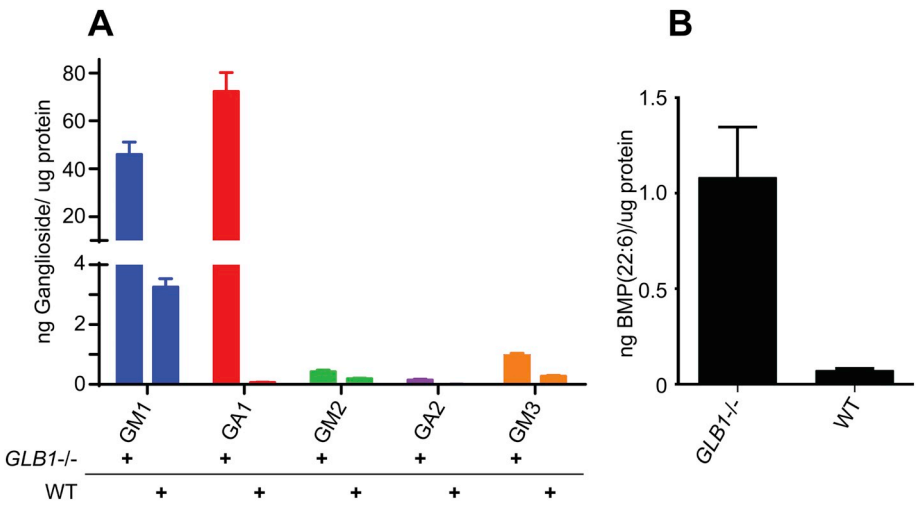


**Fig. 3.** Ganglioside and BMP(22:6) profiling for *GLB1* null and age/gender-matched normal control mouse brain extracts. The relative steady state levels of gangliosides and BMP phospholipid were determined for a brain sample taken from a *GLB1*$^{-/-}$ mouse and an age and gender-matched (7-month-old female) wildtype control. (A) Quantitative LC/MS/MS ganglioside profiling showing the indicated gangliosides as ng per μg protein of brain water homogenate for both *GLB1* null (*GLB1*$^{-/-}$) and wild type control (WT). The mean of three separate analyses are shown with error bars indicating standard deviation. (B) Bis(monoacylglycero)phosphate (22:6) levels expressed relative to a BMP (14:0/14:0) internal standard for both *GLB1* null and wild type controls and expressed as ng BMP per μg protein. The mean of three separate analyses are shown with error bars indicating standard deviation.

chains discussed above and BMP(22:6) phospholipid in acidic methanol extracts of brain homogenates. The results for a 7-month-old *GLB1* null female mouse (Fig. 3A) show a 14-fold increase in GM1 levels compared to an age and gender-matched normal control. Since only a very small amount of GA1 was observed in the wild type mouse we analyzed, the increase in GA1 steady state levels observed in the affected mouse was far greater, on the order of 486-fold. Comparing the levels of BMP (22:6), we found a 15-fold increase in the affected brain sample over that detected in the control (Fig. 3B). These results are consistent with the genotype of this animal model [27].

### *3.2. Liquid chromatography/mass spectrometry analysis of brain homogenates from GLB1 null mice showed the disease-related accumulation of water soluble glycan metabolites*

Consistent with the role played by β-galactosidase in the degradation of multiple glycans including those found in glycoproteins (Fig. 1), a number of previous studies have shown the accumulation of free glycan metabolites resulting from GLB1 deficiency. Many of these earlier studies relied on thin layer chromatography (TLC), capillary electrophoresis, or liquid chromatography to detect these species and for subsequent biochemical analysis for structural characterization [3–6,11,12,14,16,18]. Using these methods, most of these soluble glycans were shown to be metabolites of N-linked glycans originating from glycoproteins. More recently, mass spectrometry based methods have been employed resulting in the discovery of even more of these types of metabolites [7–10,13,15,17,19]. However, most of the MS studies utilized direct sample introduction methods such as direct injection-ESI and MALDI to detect these free glycans and consequently they were not able to differentiate between isobaric species that may be present. Furthermore, data-dependent tandem mass spectrometry, a very useful means of characterizing and distinguishing between different isobars based on their unique product ion profiles, could not be effectively used without separation as part of the workflow. Consequently, the diversity of these kinds of metabolites in GM1 gangliosidosis has likely been under reported.

In order to gain further insights into the kinds of metabolites that accumulate and may contribute to the progression of disease in GM1 gangliosidosis, we carried out a comprehensive analysis of glycan metabolites. In order to account for a large number of isobaric species as well as species with unique *m/z* values, we used forward phase amide-column chromatography/mass spectrometry (FPAC-LC/MS). To gain structural information, especially of multiple isobars, we used data-dependent MS/MS with the ions of interest undergoing product ion fragmentation by collision induced dissociation (CID). We analyzed soluble glycans present in homogenized tissues or biological fluids such as urine. The aqueous supernatant from these homogenates were clarified by centrifugation and the glycans present in the supernatants were end-labeled with aniline by reductive amination and subsequently analyzed by Glycan Reductive Isotope Labeling LC/MS (GRIL-LC/MS) as described in the Materials and Methods section. This method labels the reducing end of oligosaccharides with aniline allowing the detection of reducing sugar species including incompletely degraded glycan metabolites that accumulate in GM1 gangliosidosis. The aniline tag also helps orient labeled molecules in the data-dependent MS/MS spectra by relating the product ions to both the NRE and the reducing end of each parent ion.

We first compared brain water homogenates made from 7-month-old *GLB1* null and normal control mice. In the affected sample we detected a number of aniline-labeled species consistent with soluble glycan metabolites (Fig. 4). Little or no trace of any of these glycan metabolites was detected in the age-matched normal control mouse brain consistent with these species being disease-related substrates for β-galactosidase (Fig. 4, bottom trace). In the *GLB1* null sample, we observed oligosaccharides ranging in size from trisaccharides (dp3) to dodecasaccharides (dp12) many of which were part of isobaric series (Fig. 4 and Supplemental Fig. 2). The most abundant ion detected has an *m/z* value (988.4) consistent with a pentasaccharide (dp5) composed of three hexose (Hex) residues and two *N*-acetyl hexosamine (HexNAc) residues ($Hex_3HexNAc_2$). A number of other dp5 isobaric species were also observed. Data-dependent MS/MS analysis of the most abundant ion detected two product ions formed by the neutral loss of either a single Hex or HexNAc residue from the end opposite the aniline-tagged reducing end. This suggests a biantennary parent ion with two distinct NRE residues (Supplemental Fig. 3). These results are consistent with the most abundant dp5 ion being a mucin-type O-linked glycan metabolite which has not been previously described in the literature. The N-linked dp5 glycan metabolite if present should have the sequence, starting from the NRE, Gal-GlcNAc-Man-Man-GlcNAc (Supplemental Fig. 4B, bottom panel). This N-glycan structure has only one NRE (β-linked galactose) and will generate just one product ion after the neutral loss of a monosaccharide from that end. On the other hand, Core 1 and Core 2 O-linked glycan metabolites can have two NRE residues (Supplemental Fig. 3, Supplementary Fig. 4). This is especially true for Core 2 species which have the base structure Gal-GalNAc-GlcNAc with the reducing end being the bridging GalNAc. Careful examination of the full product ion profile for this dp5 species gave consistent results with either a Core 1 species with the general structure Gal-(GlcNAc)Gal-Gal-GalNAc or a Core 2 species with the general structure $Gal_2$-Gal-(GlcNAc)GalNAc (Supplemental Fig. 3).

In total we detected nine isobars with *m/z* = 988.4, seven of which showed similar product ion profiles consistent with Core 1 and Core 2

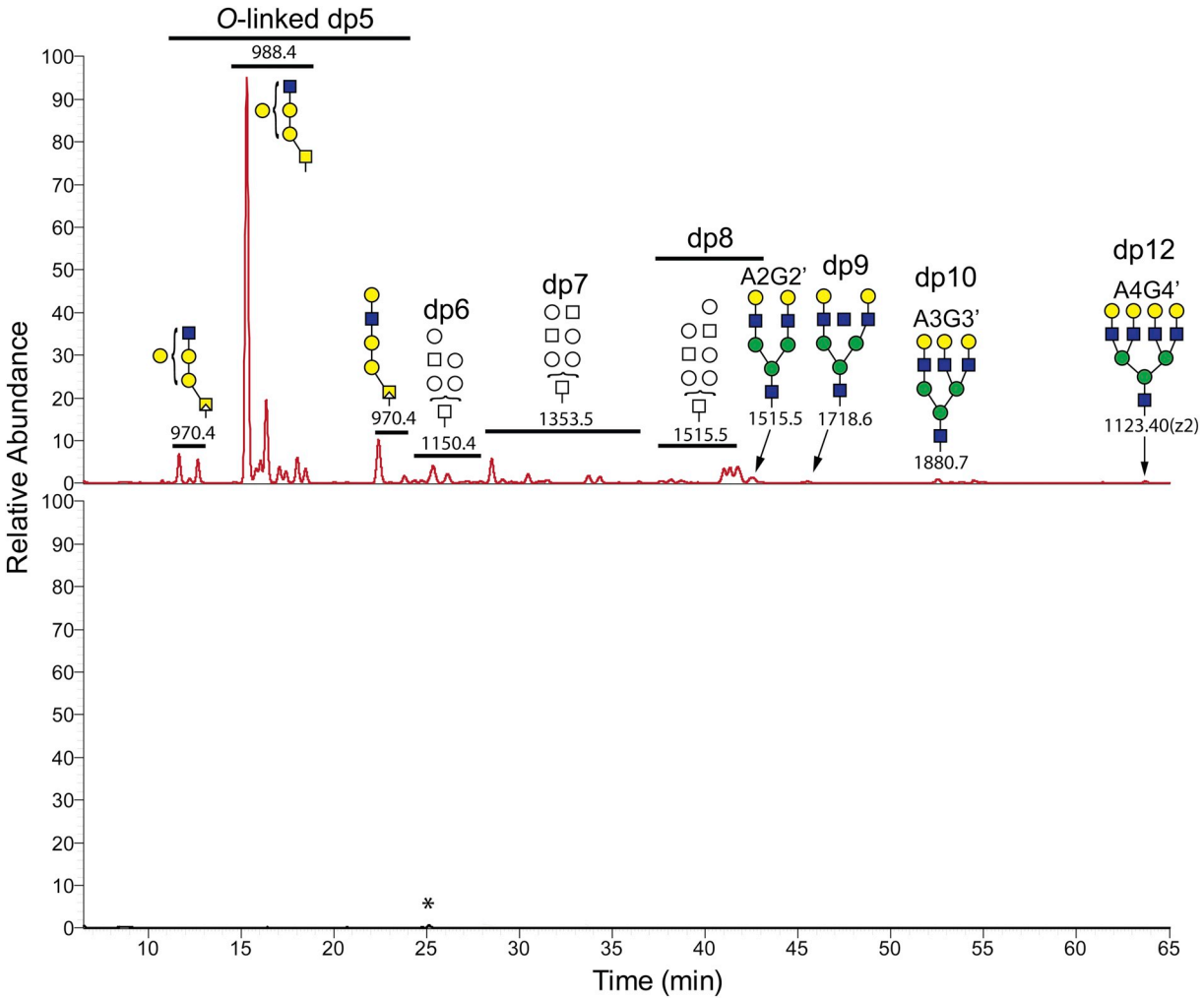


**Fig. 4.** Soluble oligosaccharide metabolites in water homogenates from *GLB1* null and wild type mouse brains. The soluble fraction from mouse brain homogenates was end-labeled with aniline as described for the GRIL-LC/MS method in the Material and Methods section to detect reducing sugars. Labeled products were separated by forward phase amide column chromatography and species with *m/z* values consistent with labeled oligosaccharides were detected by MS. The traces for the *GLB1* null brain sample and the corresponding normal control were normalized to $6 \times 10^5$ arbitrary ion intensity units for comparison. The degree of polymerization (number of monosaccharides in each oligosaccharide) is also shown (dp number) as well as putative oligosaccharide structures based on *m/z* values, retention times, and available product ion profiles. The top panel shows the results from a 7-month-old $GLB1^{-/-}$ mouse brain with different oligosaccharides ranging in size from pentasaccharides (dp5) to dodecasaccharides (dp12). Glycans that are putative metabolites deriving from mature A2G2, A3G3, and A4G4 N-linked glycans are indicated using a prime symbol to the left (A2G2', A3G3', and A4G4'). Also shown is a series of pentasaccharides (dp5) with CID data consistent with O-linked sugars that includes the most abundant glycan metabolite detected. The bottom panel shows the corresponding results for a 7-month-old normal mouse brain control. The small peak (starred) in the chromatogram does not have an *m/z* value that corresponds to a glycan and is likely a contaminant.

O-linked glycans and likely represent different branching variants. The other two dp5 exhibit product ion profiles having just a single NRE and are thus consistent with non-branched structures. These could be either a linear extended O-linked Core 1 structure or the previously described Gal-GlcNAc-Man-Man-GlcNAc dp5 species [8,15] (with the two mannose residues linked by either an α1–3 linkage or a α1–6 linkage, see Fig. 1).

Besides the dp5 isobaric series, we also detected multiple isobars for hexasaccharides dp6($Hex_4HexNAc_2$), heptasaccharides dp7($Hex_4HexNAc_3$), and octasaccharides dp8($Hex_5HexNAc_3$) (Supplemental Fig. 2). However, many of the oligosaccharides larger than dp5 had lower ion intensities which resulted in incomplete CID spectra and consequently less structural information could be determined from the product ions formed. A number of the dp6 and dp7 isobaric species did exhibit product ion spectra suggesting two different NRE termini but the limited CID spectra for these larger oligosaccharides is compatible with both N-linked and O-linked structures. Because of the number of isobars for each oligosaccharide size class (Supplemental Fig. 2): eight for dp6, eleven for dp7, and six for dp8, it is likely that both N-glycans and O-glycans are present. The composition of the dp8 isobars ($m/z$ = 1515.5) is consistent with the previously observed metabolite deriving from the complex N-linked glycan structure A2G2 (Oxford notation, see Fig. 1) which is a common glycan seen in glycoproteins. For clarity, we used the prime symbol to distinguish metabolites from the parent oligosaccharide from which they are derived. For example, A2G2' is the β-galactosidase substrate metabolite that derives from A2G2 and differs from it by the loss of the first reducing end GlcNAc (Fig. 1). Larger oligosaccharides with *m/z* values consistent with metabolites for A3 and A4 glycans were also detected but were assigned based only on *m/z* value and retention time without benefit of CID data because of their low ion intensities (Fig. 4).

In order to gain more insight into the structure of these soluble glycan metabolites, the soluble glycan fraction was subjected to enzymatic removal of non-reducing end galactose with recombinant β-galactosidase and the resulting remnant structures were analyzed by the same method used to detect and characterize the glycan metabolites

**Table 1**
Glycan metabolites detected in *GLB1* null mouse brain. The *m/z* values, monosaccharide composition, putative structures, likely type of glycoprotein linkage, and the number of isoforms detected in a 7-month-old *GLB1*$^{-/-}$ mouse brain are shown. Insufficient ion recovery for the four largest oligosaccharide glycoforms resulted in their assignment made by *m/z* value and retention time alone (star).

| *m/z* value | Formula | Putative Structure | Type | Isoforms |
|---|---|---|---|---|
| 623.2 | dp3(1HexNAc,2Hex) | 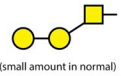 (small amount in normal) | O | 2 |
| 785.3 | dp4(1HexNAc,3Hex) | 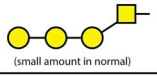 (small amount in normal) | O | 2 |
| 970.4 | dp5(1HexNAc, 1dehydro-HexNAc,3Hex) Biantennary | 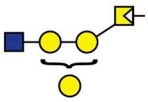 | O | 3 |
| 970.4 | dp5(1HexNAc, 1dehydro-HexNAc,3Hex) | 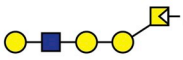 | O | 2 |
| 988.4 | dp5(2HexNAc,3Hex) Biantennary | 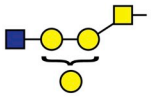 | O | 7 |
| 988.4 | dp5(2HexNAc,3Hex) | 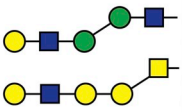 | E | 2 |
| 947.4 | dp5(1HexNAc,4Hex) | 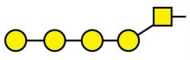 (small amount in normal) | O | 2 |
| 1150.4 | dp6(2HexNAc,4Hex) | 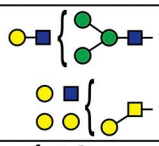 | E | 8 |
| 1353.5 | dp7(3HexNAc,4Hex) | 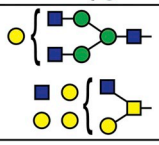 | E | 11 |
| 1218.5 | Oligosaccharide moiety Biantennary | ND | # | 1 |

| *m/z* value | Formula | Putative Structure | Type | Isoforms |
|---|---|---|---|---|
| 1515.5 | dp8(3HexNAc,5Hex) | 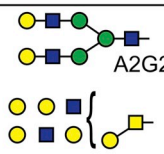 A2G2' | E | 6 |
| 1718.6 | dp9(4HexNAc,5Hex) | 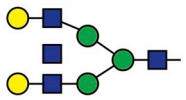 | N | 2 ★ |
| 1880.7, 940.8(z2) | dp10(4HexNAc,6Hex) | 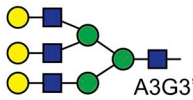 A3G3' | N | 2 ★ |
| 1042.4(z2) | dp11(5HexNAc,6Hex) | 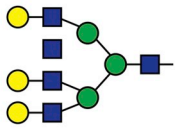 | N | 2 ★ |
| 1123.4(z2) | dp12(5HexNAc,7Hex) | 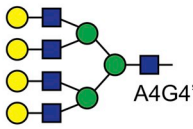 A4G4' | N | 1 ★ |

★ = No CID confirmation
O = O-linked glycan metabolite
N = N-linked glycan metabolite
E = Either type of glycan metabolite
# = Non-reducing oligosaccharide or glycoconjugate with CID data consistent with

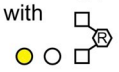

ND = Structure not fully determined

accumulating in the *GLB1* null mouse brain. The resulting remnant structures (Supplemental Fig. 4A) allowed us to restrict the pool of possible structures for the soluble glycans accumulating in the knockout mouse (Supplemental Fig. 4B).

From all of these results we were able to compile a table of the oligosaccharide metabolites we detected in the *GLB1*$^{-/-}$ mouse brain, including the total number of isobaric forms, and their putative structures (Table 1). A total of 56 distinct oligosaccharide structures based on retention time, mass, and product ion profile were observed. In addition to the oligosaccharide species labeled with aniline at their reducing end, we detected a single species with *m/z* value = 1218.5 which appears to be a non-reducing oligosaccharide or an intact glycoconjugate since differential isotope labeling with both [$^{13}C_6$]Aniline and [$^{12}C_6$]Aniline failed to produced differentially isotope-labeled products. However, daughter ions consistent with the neutral loss of two Hex and two HexNAc residues suggests this disease-related species is or originates from a glycoconjugate (Table 1).

Thus, we have detected a diverse group of soluble glycan metabolites in GLB1 deficient mouse brain including a number of Core 1 or Core 2 mucin type O-linked glycans which have not been previously described. One of these O-glycan metabolites, a pentasaccharide, is part of an isobaric dp5 series and has the largest abundance of any of the glycan metabolites detected in affected mouse brain suggesting that, if like gangliosides, glycan metabolite accumulation drives certain aspects of disease, it may play an important role in the progression of GM1 gangliosidosis.

### *3.3. Disease-related soluble glycan metabolites are detected in a number of different tissues and biological fluids in β-galactosidase deficient mice*

In order to determine if oligosaccharide metabolites similar to those detected in brain also accumulate in other tissues in the *GLB1* null mouse, we screened for soluble glycans in liver, spleen, kidney, and urine samples. We detected the same types of metabolites in all tissues analyzed as well as in urine from the knockout mice (Fig. 5). Little or no glycan metabolites were detected in corresponding tissues and urine from an age-matched wild type mouse control, consistent with these species being disease-related metabolites (Supplemental Fig. 5). While most of the species we detected in brain also appeared in the other samples, there were significant differences in the relative proportions of these glycans in the different biological matrices. For example, the O-linked pentasaccharide isobaric series ($Hex_3HexNAc_2$ – eluting between

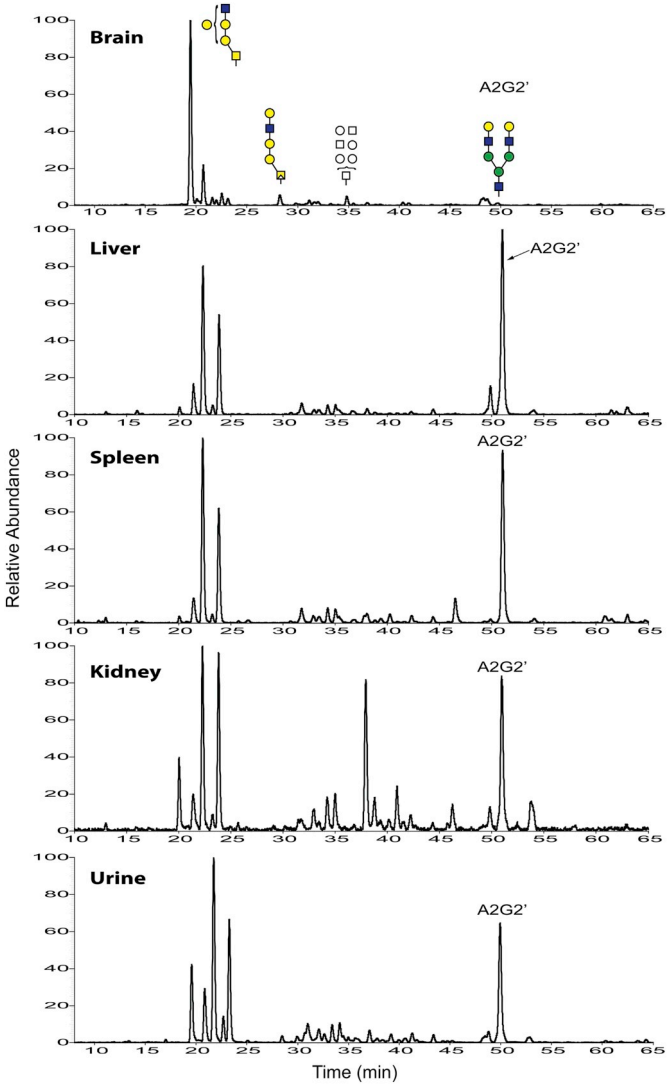


**Fig. 5.** Soluble free glycan metabolites in various tissue homogenates and urine from a *GLB1* null mouse. Soluble glycans were extracted from a 7-month-old β-galactosidase deficient mouse and end labeled with aniline as described in the Methods section. Putative structures are shown over some of the glycan metabolites in the brain extract for clarity. The putative N-linked A2G2' metabolite is also indicated. Tissue glycans were injected at 70 µg protein equivalents while the urine samples were injected at 20 µL neat volume equivalents. Ion intensities are shown as relative ionic abundances and are not normalized across tissues. Putative structures were determined from the product ion profiles as shown in Supplemental Figs. 3 and 6.

20 and 24 min) was detected in all samples tested. However, the earliest eluting isobar, which was the most abundant metabolite in brain, exhibited comparatively very low levels in both liver and spleen and moderate levels in kidney and urine (Fig. 5). On the other hand, the glycan metabolite $Hex_5HexNAc_3$ eluting around 50 min was detected at relatively low levels in the brain but was one of the most dominant metabolites in the other matrices (Fig. 5). And finally, a dp7 species, eluting at just over 37 min, was one of the most dominant metabolites in kidney but was detected at significantly lower levels in the other matrices (Fig. 5). Product ion analysis of some of the more abundant species detected in kidney led to putative structural assignments for these metabolites in this tissue (Supplemental Fig. 6). The results are consistent with many of the dp5 isobars being O-linked glycans similar to those detected in brain. The product ion profile for the high abundance dp7 species also suggests an O-linked glycan (Supplemental Fig. 6E). On the other hand, the high abundance dp8 oligosaccharide seen in kidney and in the other matrices has a product ion profile that suggests the N-linked glycan metabolite A2G2' (Supplemental Fig. 6F).

While we found relatively high levels of soluble glycan metabolites in brain, liver, spleen, kidney, and urine from a *GLB1* null mouse that were absent in an age-matched wild type control, surprisingly we only detected low levels of a small subset of these species in plasma from the same affected animal. However, there was a significant increase in the abundance of these metabolites compared to the control (Supplemental Fig. 5). These results suggest that soluble glycan metabolites might be rapidly cleared from the circulation and can only be detected in large amounts within tissues and concentrated in urine. Alternatively, these differences may be due to a dilution effect (only 1–2 µL plasma analyzed compared to 20 µL urine).

Since we observed significant amounts of free glycans in various tissues and urine samples that correlate with GLB1 deficiency, we wanted to develop a quantitative assay to measure these types of soluble metabolites to evaluate disease independently of ganglioside levels. Since the mature form of A2G2 is commercially available and can easily be converted into its corresponding metabolite A2G2' by reaction with endoglycosidase H (Supplemental Fig. 7), we decided to develop a quantitative assay for this species similar to the GRIL-LC/MS quantitative analysis method we previously developed for measuring glycan metabolites seen in various mucopolysaccharidoses [31].

Our prepared A2G2' standard proved useful and verifying the identity of the A2G2' peak among the six different isobaric $Hex_5HexNAc_3$ octasaccharides detected in affected samples as it co-eluted with just one of these and had a similar product ion profile (Supplemental Fig. 7B). Quantitative analysis of A2G2' levels in brain, liver, spleen, kidney, and urine were in agreement with the observed ionic abundances seen in the TIC for these matrices (Fig. 5). Compared to the peripheral samples, brain samples exhibited the lowest steady state levels of A2G2' with < 20 pmole A2G2'/mg protein compared to almost 1000 pmole A2G2'/mg protein in liver (Fig. 6). Interestingly, while there was approximately a 40-fold increase in A2G2' levels between wildtype and affected spleen, the wildtype levels in spleen were higher than in all other matrices and were in fact similar to those seen in affected brain (Fig. 6).

### *3.4. Both gangliosides and disease-related glycan metabolites increase with age in GLB1 null mice but not in wildtype mice*

Consistent with previously published results for this mouse model [27], we observed increasing accumulation of ganglioside storage in the brains of affected mice as they age (Fig. 7A). High levels of both GM1 and its corresponding asialo derivative, GA1, were detected at 1 month of age in *GLB1* knockout mice compared to wild type controls which showed only low levels of GM1 and no detectable GA1. At 4 months of age both GM1 and GA1 steady state levels were elevated compared to 1-month-old *GLB1* null mice. No significant difference in GM1 levels between 1 month and 4 month mice was observed in normal controls. Steady state levels for GM1 and GA1 increased further by 7 months in the knockout mouse while GM1 levels were not significantly changed in the wild type mice. At none of the ages tested did normal control mice exhibit significant levels of GA1 accumulation and only exhibited low levels of GM1 (Fig. 7A). Comparing GM1 levels in the *GLB1* null mice and normal controls throughout the natural history study, GM1 levels were approximately 9-fold higher in the knockout mice at 1 month, while at 7 month the levels in affected mice were approximately 14 times higher.

Analogous to the progressive increases in ganglioside steady state levels observed in *GLB1* null mice as they age, brain levels of soluble A2G2' glycan also showed increases (Fig. 7B). However, unlike both GM1 and GA1 gangliosides, which showed a steady increase, the A2G2' levels didn't exhibit a significant change between 1 and 4 months but did show a significant increase between 4 and 7 months of age. In all cases, A2G2' levels were below the limit of detection in age-matched

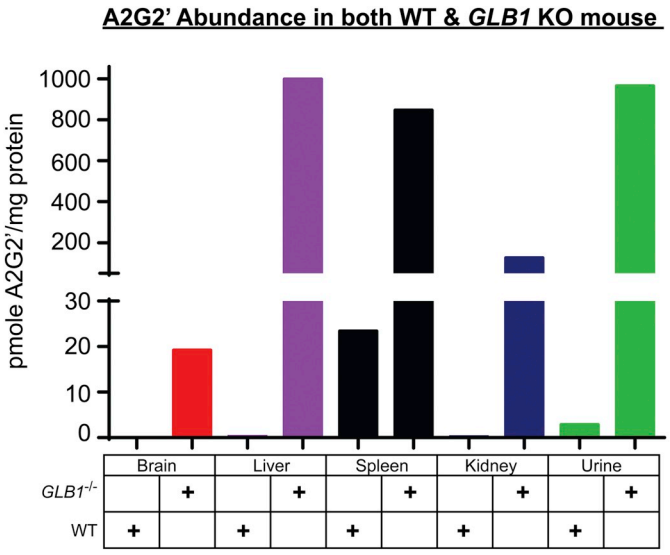


**A2G2' Steady State Levels**

| Genotype | Tissue | Results | Units |
|---|---|---|---|
| WT | Brain | 0.0 | pmole/mg protein |
| KO | Brain | 19.24 | pmole/mg protein |
| WT | Liver | 0.27 | pmole/mg protein |
| KO | Liver | 998.76 | pmole/mg protein |
| WT | Spleen | 23.43 | pmole/mg protein |
| KO | Spleen | 845.86 | pmole/mg protein |
| WT | Kidney | 0.15 | pmole/mg protein |
| KO | Kidney | 125.16 | pmole/mg protein |
| WT | Urine | 2.90 | pmole/100ul urine |
| KO | Urine | 965.52 | pmole/100ul urine |

**Fig. 6.** A2G2' metabolite steady state levels in various tissues and urine from age-matched *GLB1* null and normal wildtype control mice. A2G2' steady state levels in various tissue samples and in urine where compared between wild type and *GLB1* null mice. Steady state A2G2' levels are expressed as pmole A2G2' per mg protein in clarified tissue homogenate and urine. Numeric results are also shown in the table to the right.

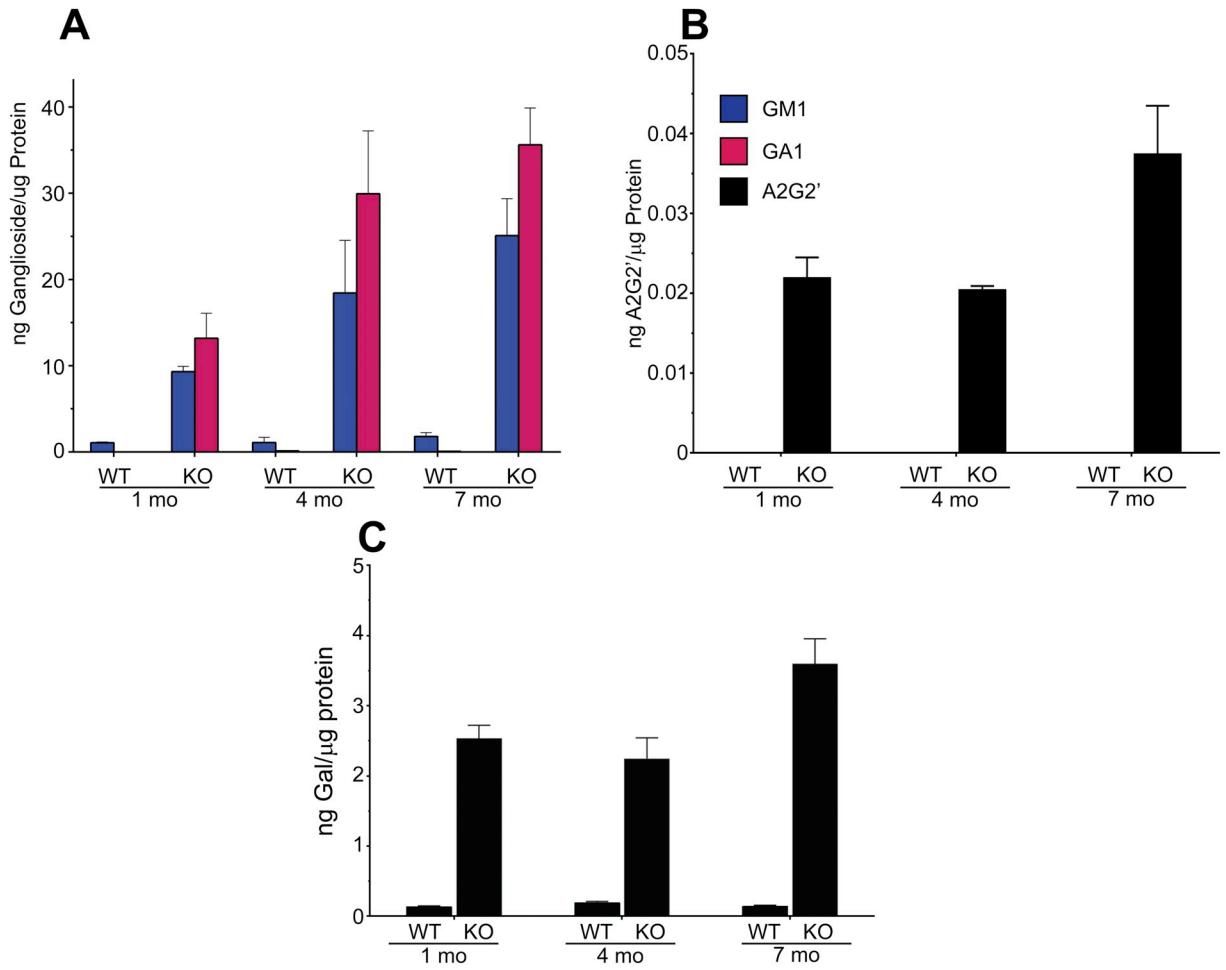


**Fig. 7.** Natural history study of gangliosides and soluble oligosaccharide metabolites in the brain of *GLB1* null and normal control mice. A. GM1 (blue bars) and GA1 (red bars) levels in brain homogenates from 1, 4 and 7-month-old *GLB1* null and age-matched normal control mice. Values are normalized to µg protein equivalents and are the mean of three animals for each time point, +/− SD. B. Corresponding A2G2' brain levels in 1, 4, and 7-month-old null and normal control mice ($n$ = 3, +/− SD). Values are normalized to µg protein equivalents. C. Corresponding total enzyme-released galactose in 1, 4, and 7-month-old *GLB1* null and normal control mice (n = 3, +/− SD). Values are normalized to µg protein equivalents.

wild type controls.

Despite observing increased steady state levels of both gangliosides and glycan metabolites, we noticed that the amounts of gangliosides accumulating in *GLB1*$^{-/-}$ mouse brain tissue far outpaced those of A2G2'. For example, by 7 months, we detected 25 ng of GM1 per μg protein and only 0.037 ng A2G2' per μg protein, almost a 700-fold difference. However, comparing the relative abundance of A2G2' in *GLB1* null mouse brain to the rest of the glycan metabolites observed (Fig. 4) and seeing that A2G2' is far less abundant in brain compared to other tissues (Fig. 5), A2G2' levels vastly underestimate the accumulation of free glycans in the brains of knockout mice.

In order to more faithfully compare the amount of gangliosides and glycan metabolites that accumulate in disease, we measured the total amount of non-reducing end β-linked galactose present in the aqueous fraction of brain homogenates from affected and wildtype mice at 1, 4, and 7 months of age. Soluble glycans purified from these samples were treated with recombinant β-galactosidase enzyme and the released galactose quantified using ion chromatography and pulsed amperometric detection (PAD) (Supplemental Fig. 8). The observed pattern of increasing enzymatically-released galactose accumulation with age was very similar to that of A2G2' alone, thus justifying its use as a surrogate for total disease-related glycan metabolites (Fig. 7B and C). In normal control mice, where A2G2' levels were below the limit of detection, galactose levels were detectable at relatively low levels after β-galactosidase treatment. Galactose levels were far higher in all of the affected samples tested.

Comparing the total amount of gangliosides with the total amount of liberated galactose can be useful since much of this galactose is from the non-reducing ends of glycan metabolites. Therefore, these galactose levels are a good stoichiometric estimate of these metabolites when internal standards such as the one used for A2G2' are not available. For example, at 7 months of age, approximately 3.7 ng galactose/μg protein was detected in *GLB1* null mouse brains (Fig. 7C). If we assume that most of the glycan metabolites are dp5 and have two NREs per glycan as suggested by our product ion analysis results, then with the molecular weight of galactose being 180 Da, approximately 0.01 nmoles of dp5 were detected. The molecular mass of dp5 is 910 Da which equates to 9.1 ng glycan metabolite per μg protein detected. Comparing this to approximately 26 ng of GM1 in the same samples, the estimated glycan levels are significant. In other tissues where ganglioside accumulation is negligible, glycan accumulation may be very important for disease progression involving those tissues. Finally, since gangliosides are not normally detected in an important non-invasive sample matrix such as urine but glycan metabolites are, we decided to use free glycan analysis as our primary biomarker assay for this disease.

### 3.5. Both gangliosides and disease-related glycan metabolites are elevated in GLB1 deficient human brain tissue and urine suggesting similar patterns of β-galactosidase substrate accumulation in both affected mice and humans

After observing a variety of glycan metabolites including what appear to be newly discovered O-glycans accumulating in *GLB1* null mice, we wanted to investigate if a similar constellation of N-glycan and O-glycan metabolites also accumulate in human GM1 gangliosidosis patients.

We obtained post mortem brain samples (cerebral cortex) collected from an affected patient and two normal controls and subjected these to glycolipid analysis. RNA sequencing indicated that the affected human had mutations c.765G > C (p.Gln255His) and c.335A > C (p.His112Pro) in the *GLB1* gene locus. In comparing the relative abundance of GM1 acyl-isoforms present in the human samples, we found the same pattern we observed in mice with GM1(d18:1/18:0) and GM1(d18:1/20:0) contributing to most of the ganglioside ion intensity. We carried out ganglioside and BMP phospholipid profiling as we did before with murine samples. As expected, we found both GM1 and the corresponding asialo derivative, GA1, as well as BMP-phospholipid were elevated in the human GM1 gangliosidosis brain sample compared to the normal brain samples (Fig. 8).

We next carried out soluble glycan analysis of water homogenates made from these human brain samples. Consistent with our results in mouse brain tissues (Fig. 4), we found similar types of glycan metabolites in the human GM1 gangliosidosis patient brain but not in the unaffected controls (Fig. 9) including a number of isobaric pentasaccharides ($m/z$ = 988.4). Many of these dp5 species gave CID product ion spectra consistent with metabolites derived from mucin type extended Core 1 or 2 O-linked glycans (Supplemental Fig. 9). Interestingly, the most dominant dp5 isoforms in the human patient did not coincide with the most dominant isoform detected in mouse brain (compare Fig. 4 with Fig. 9) which may be due to species differences.

In addition to the dp5 isobaric series, various larger glycan metabolites were also detected including multiple dp6 ($m/z$ = 1150.4), dp7 ($m/z$ = 1353.5), and dp8 ($m/z$ = 1515.5) oligosaccharides. For many of these larger glycan isoforms, structural evaluation using CID failed to determine if they derived from either N- or O-linked glycans. An exception was A2G2' which was structurally identified by having the same retention time and similar product ion spectra as that of the A2G2' internal standard. Larger oligosaccharides (dp9 and dp10) were inferred to be metabolites derived from A3G2 and A3G3, based on their $m/z$ values and retention times (the two putative structures shown to the right of A2G2' in the top panel of Fig. 9A).

Quantitative analysis of A2G2' steady state levels in both affected and unaffected brain samples showed A2G2' levels to be below the lower limit of detection in the unaffected controls. However, in the GM1 gangliosidosis patient, we observed A2G2' levels to be largely elevated in comparison (Fig. 9B). However, as we observed in *GLB1* null mice, increases in GM1 and GA1 ganglioside levels outpaced those of A2G2' (24.2 ng GM1/μg protein and 1.01 ng A2G2'/μg protein). Regardless, given the number of distinct glycan metabolites detected, when compared as a class to gangliosides, soluble glycans likely represent a large proportion of GLB1 substrates that accumulate as a result of GM1 gangliosidosis. This is exactly what we determined above for the mouse model by measuring the amount of β-linked terminal galactose present in samples (Supplemental Fig. 8).

We next looked for the presence of soluble glycans in urine samples collected from six pediatric GM1 gangliosidosis patients (Table 2) and six unaffected normal pediatric controls. In all of the GM1 gangliosidosis patients we found glycan metabolites similar to those we detected in both the GM1 gangliosidosis patient brain and the mouse model. As expected, little or no soluble glycans were detected in any of the normal controls (Fig. 10A). In the disease samples, we observed a series of dp5 oligosaccharide isobars similar to the O-glycan pentasaccharides observed in both human and mouse samples as well as comparatively high levels of larger oligosaccharides including A2G2'.

We next quantified A2G2' in these urine samples and compared the results after normalizing to creatinine levels. Urinary A2G2' levels in all of the affected patients were greatly elevated compared to the normal controls, which were at or below the limit of detection (Fig. 10B). Interestingly, a patient (P12–2363) with the mutation R59H, a *GLB1* mutation commonly found in Brazil [32,33], where all the affected urine samples were sourced, had the highest urinary A2G2' levels. This patient also exhibited significant clinical symptoms at birth (Table 2) suggesting a possible correlation between severity and biomarker levels. This observation will need to be tested in a much larger set of patient samples.

Genetic mutations effecting the *GLB1* gene can result in two clinically different diseases, GM1 gangliosidosis and Morquio B [2,20,34]. With the former having a neurodegenerative phenotype and characterized by increases in gangliosides while the latter exhibits a skeletal phenotype and is associated with increases in keratan sulfate (KS). Since significant levels of KS can be measured in normal urine, we wanted to determine if urinary KS levels are elevated in any of the six GM1 gangliosidosis patient urine samples compared to normal controls.

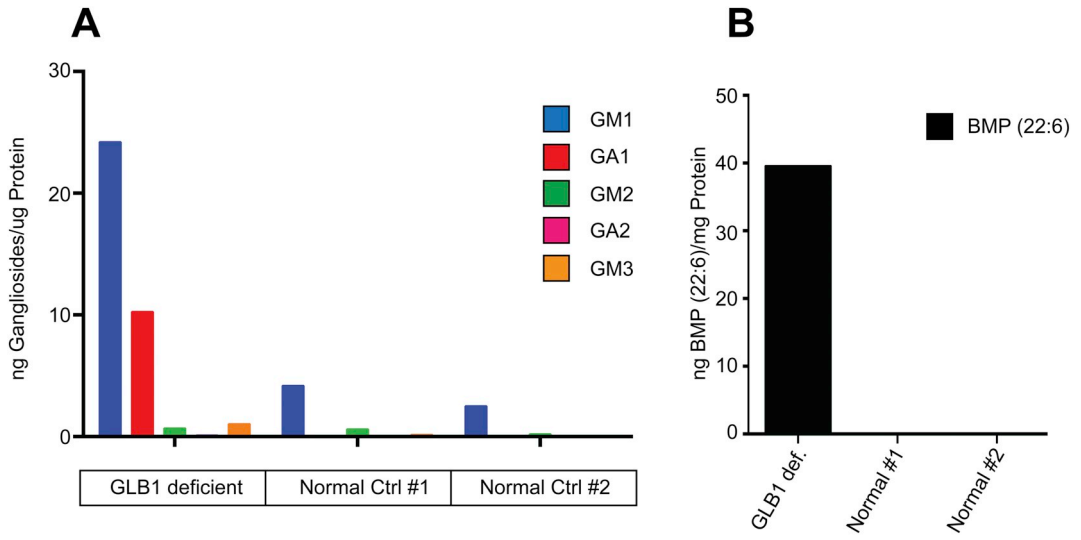


**Fig. 8.** Ganglioside and BMP-phospholipid levels in normal human and GM1 gangliosidosis patient brain homogenates. A. Ganglioside levels in human brain homogenates including a single GLB1 deficient human and two normal controls. Each ganglioside is normalized to μg protein equivalents. B. BMP-phospholipid levels normalized to mg protein equivalents.

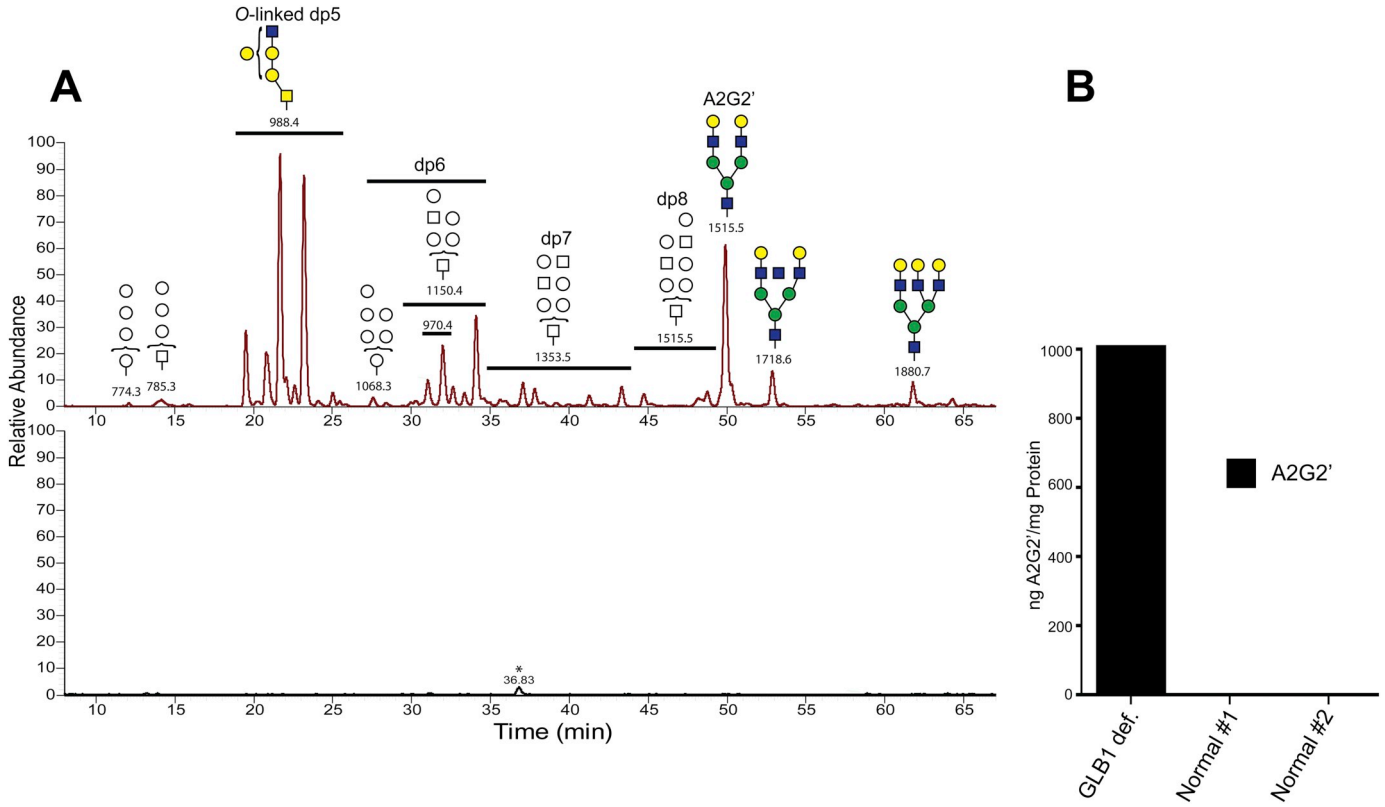


**Fig. 9.** Glycan metabolites in a human GM1 gangliosidosis patient brain homogenate. A. Soluble glycan metabolites in brain homogenates were analyzed by LC/MS and data-dependent MS/MS as previously described. Different size oligosaccharides are symbolically indicated with putative structures based on *m/z* values, available CID spectra, and retention times. The *m/z* values for each oligosaccharides are also shown. The upper panel shows the glycan metabolites in the GLB1 deficient patient while the results for one of the normal controls is shown in the bottom panel (both controls gave the same negative results for glycan metabolites). The star in the bottom panel denotes a species with *m/z* value that does not correspond to a glycan and is likely a contaminant. B. Quantitation of the A2G2' metabolite is shown for all three brain homogenates normalized to mg protein equivalents.

To carry this out we used GRIL-LC/MS in which urinary KS was first digested with keratinase II and then labeled with [$^{12}C_6$]aniline. The cumulative ion intensity for all KS digestion products for each sample was compared to one of the normal controls used as a reference sample that had been heavy isotope labeled with [$^{13}C_6$]aniline. This approach allowed us to measure relative differences in KS levels among the affected and unaffected normal controls. We chose as our reference the control sample with the highest KS levels among the six normal controls (dotted line in Fig. 10C). Only three of the patient samples had urinary KS levels significantly elevated above this level while the other three affected samples exhibited KS levels at or below this level (Fig. 10C). The patient with the highest urinary A2G2' levels also exhibited the

**Table 2**
Human GM1 gangliosidosis patients from whom urine samples were obtained. Shown are the patient identification (ID), age of urine sample collection (Age), gender, diagnosis (Dx), Age of onset (Onset), age of death (Death), clinical symptoms and disease severity (Description), and available *GLB1* genotyping results.

| ID | Age | Gender | Dx | Onset | Death | Description | Genotype |
|---|---|---|---|---|---|---|---|
| P12–2363 | 20 months | Male | GM1 type 1 | 06 months | 25 months | Hydrocele noted at birth; started investigation at the age of 6 months due to delayed milestones | R59H/unknown (only 2 mutations tested) |
| P09–0806 | 10 months | Female | GM1 type 1 | 10 months | Unknown | Coarse facies, palpebral hemangioma, global hypotonia, upper airway obstruction | Not genotyped (DNA available) |
| P07–2987 | 13 months | Male | GM1 type 1 | 13 months | Unknown | Seizures with 2 months of life, global hypotonia, delay in neuromotor development, global hypotonia | Not genotyped (no DNA available) |
| P12–3182 | 11 months | Female | GM1 type 1 | 11 months | 14 months | No data available | 1622-1627insG/ unknown (only 2 mutations searched) |
| P09–1212 | 3 months | Male | GM1 type 1 | 03 months | Unknown | Mongolic spots, hepatomegaly, cardiomegaly, inguinal hernia | Not genotyped (no DNA available) |
| P06–1901 | 10 months | Female | GM1 type 1 | 10 months | Unknown | No data available | Not genotyped (no DNA available) |

highest urinary KS levels. These results suggest that in some patients both N-glycan and KS metabolites are elevated and in other patients just N-glycans levels are increased while KS levels are not significantly affected. Neither CSF nor brain tissue samples were available from the six GM1 gangliosidosis patients so we were not able to evaluate ganglioside accumulation to compare to both A2G2' and KS levels. Despite this, our results demonstrate that glycan metabolite levels such as those for the N-glycan metabolite A2G2' correlate well with disease and may be as good a biomarker for GM1 gangliosidosis as GM1 gangliosides. Given the ease of obtaining urine samples from patients, measuring urinary glycan metabolite levels may be a more clinically relevant means of biochemically assessing disease.

## 4. Discussion

In this study we carried out a comprehensive survey of β-galactosidase substrates that accumulate in GM1 gangliosidosis by probing a related mouse model for this disease. This allowed us to develop a quantitative set of assays that assess multiple biomarkers impacted by loss of GLB1 enzyme activity and give a more complete picture of disease severity and a wider-ranging panel of endpoints with which to evaluate the efficacy of new therapeutics to treat this disease. This panel of biomarkers include a set of gangliosides and soluble glycan metabolites, each one of which contain terminal non-reducing end β-linked galactose, which is the definitive substrate for GLB1 found in a number of glycoconjugates. In addition to these primary biomarkers, we also evaluated the steady state levels of BMP(22:6) phospholipid, a secondary biomarker previously shown to be effected in gangliosidoses such as GM1 gangliosidosis [30].

In order to develop an efficient LC/MS/MS assay for gangliosides, it was necessary to determine which isoforms to measure. We used tandem mass spectrometry to determine the predominant acyl-isoforms of GM1 present in both *GLB1*$^{-/-}$ and wild type mice and found that just two isoforms, GM1(d18:1/18:0) and GM1(d18:1/20:0), contributed to almost all of the total ion intensity for this class of glycolipid in brain. This was found to be true in both murine and human samples. We therefore developed an LC/MS/MS assay to quantify just these two acyl-isoforms in biological samples to assess ganglioside steady state levels. For measuring soluble glycans, we developed a quantitative assay for one member of this type of molecule, A2G2', after establishing that most if not all glycan metabolites as well as ganglioside and BMP (22:6) levels are similarly effected by GLB1 deficiency. Thus, quantitation of A2G2' holds the promise of being an effective readout for GLB1 deficiency in tissues and more easily obtainable biological fluids such as urine where little to no gangliosides can be detected.

Because a number of different glycoconjugates might serve as substrates for GLB1-dependent degradation, it is important to assess all of the undegraded substrates that accumulate in GM1 gangliosidosis. Surveying how different metabolites are effected in different tissues may lead to a better understanding of what drives disease and how disease progresses in different organs and tissues. Along those lines, besides developing comprehensive assays to assess the efficacy for new therapeutics, another motivation for carrying out this study was to discover alternative GLB1 substrates that may play important roles in this disease.

Krabbe disease (OMIM 245200) is a rare autosomal recessive lysosomal storage disorder caused by deficiency of galactocerebrosidase (GALC, EC 3.2.1.46) activity leading to the accumulation of the cerebroside galactosylceramide. Krabbe is a severe and often fatal neurodegenerative disease in children [2]. Like GLB1, GALC, is a β-linked galactosidase that acts on terminal galactose directly linked to sphingolipids. Interestingly, GALC deficiency also leads to the accumulation of the globoside lactosylceramide consistent with this species also being a substrate for the GALC enzyme [35,36]. Given that multiple glycolipids accumulate in Krabbe, we wanted to assess if a similar pattern existed in GM1 gangliosidosis. We carried out lipidomic surveys in

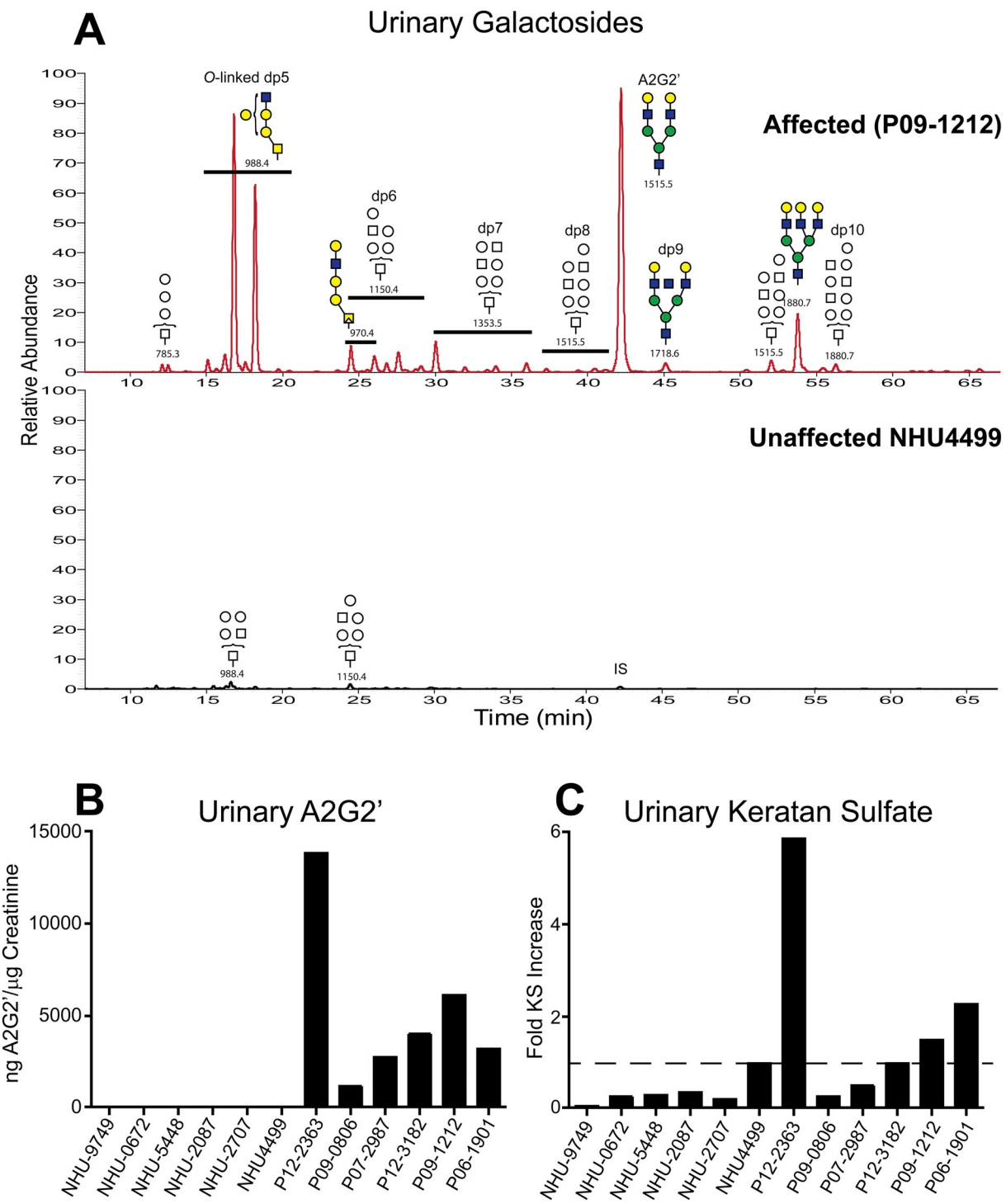


**Fig. 10.** Urinary A2G2' and keratan sulfate levels compared between human GM1 gangliosidosis patients and normal unaffected controls. Urine from six normal pediatric subjects (NHU) and from 6 affected patients diagnosed with infantile GM1 gangliosidosis (P) were analyzed for urinary A2G2' and KS. A. Representative results showing the extracted ion current for soluble glycan metabolites in urine from an affected pediatric patient, P09–1212, (top trace) and a normal pediatric control, NHU4499, (bottom trace). Putative structures for the glycans are shown along with their *m/z* values and corresponding oligosaccharide sizes (dp). All six affected patients showed similar results. The normal control exhibited only trace amounts of dp5 and dp6 oligosaccharides as well as the added A2G2' internal standard (IS). All of the normal pediatric controls exhibited similar results. B. Urinary A2G2' levels in six normal pediatric and six GM1 gangliosidosis pediatric patient urine samples normalized to creatinine levels. C. Keratinase II digestion products were labeled with [$^{12}C_6$]aniline and mixed with keratinase II digestion products from one of the normal controls (NHU4499) differentially isotope labeled with [$^{13}C_6$]aniline. Ion abundances for KS digestion products were summed together and the aggregate results normalized to creatinine levels. The fold increase in the cumulative abundances was determined ratiometrically against those of the spiked heavy isotope control reference. One-fold increase is denoted by the dotted line.

search of alternative glycolipid substrates that like GM1 and GA1 gangliosides are also effected by GLB1 deficiency and might play a role in disease progression. Our lipidomics screen only detected in the *GLB1*$^{-/-}$ mouse the accumulation of GM1, GA1, and BMP(22:6). We did not detect significant increases in lactosylceramide, galactosylceramide, sulfatides, or monogalactosyldiacylglycerol levels in the *GLB1*

null mouse, consistent with these galactosyl-lipids being substrates for other β-linked galactosidases and not for GLB1.

In comparing the relative increases we observed between sialidated GM1 and asialo GA1 gangliosides, the greatest level of increase was for GA1 species. In the unaffected normal sample, GA1 levels were at or near negligible levels, suggesting that much of the GA1 we see accumulating in affected samples results from secondary storage. This is consistent with a model for lessening of the GM1 burden in affected cells by conversion of GM1 to GA1 by the action of lysosomal sialidase activity. We saw this pattern in both murine and human samples demonstrating its importance across different species.

In addition to glycolipids, a number of previous studies have demonstrated the significant accumulation of soluble (free) glycan metabolites in various gangliosidoses including GM1 gangliosidosis [3–16,19,37]. These results suggest that GM1 gangliosidosis might be more accurately described as an oligosaccharidosis which effects the degradation of multiple glycoconjugates including gangliosides and glycoproteins. The vast majority of these previously characterized disease-related soluble glycans were found to be metabolites derived from incompletely degraded N-linked glycans such as A1G1, A2G2, A3G3, and A4G4. We analyzed the soluble fraction of tissue homogenates and urine samples and observed many of these same N-glycan metabolites from affected mice and humans. However, little or no signs of these species were detected in unaffected controls demonstrating the correlation with disease exhibited by these metabolites. Many of the previous studies showing the existence of these soluble glycans were limited by the use of either liquid chromatography without mass spectrometry or direct infusion methods such as MALDI and ESI which cannot distinguish between isobaric species. Using a more comprehensive method of glycan analysis, GRIL-LC/MS and data-dependent CID, we were able to isolate and structurally elucidate a variety of different isobaric species that included both N-linked and O-linked glycan metabolites. We detected a number of different isobaric series including series for dp5, dp6, dp7, dp8, and larger oligosaccharides. Of particular interest is a pentasaccharide series that had the general structure $Hex_3HexNAc_2$ and contributed to a large part of the total ion intensity for glycan metabolites in affected samples. We detected at least nine of these pentasaccharide isobaric species with the structure $Hex_3HexNAc_2$ ($m/z$ value of 988.4). Most of these dp5 isobars exhibited product ion profiles consistent with mucin type extended core 1 or 2 O-linked glycans. These species have not been previously described. In fact, only a few O-linked glycan metabolites have been previously observed and these were no larger than a tetrasaccharide. The large contribution to the total ion intensity by the dp5 glycan metabolites we detected suggests that they may play an important role in this disease. These species were detected in multiple tissue and urine taken from *GLB1* null mice and affected human patients with the only difference being differences in the relative ion intensity between unique dp5 isobars. Since it was outside the scope of this study, we did not attempt to structurally elucidate these species any further. It will be important for future studies to do a more complete structural determination of these isobars to help determine their importance in different tissues and longitudinally in afflicted patients. Their structural elucidation may also facilitate the synthesis of standards for their quantification by LC/MS methods.

The N-glycan metabolite A2G2' was chosen as a surrogate glycan biomarker because its levels are affected by GLB1 deficiency similarly to those of other glycan metabolites. Furthermore, it was possible to generate the corresponding standard by enzymatic removal of the reducing end GlcNAc from its precursor oligosaccharide in defined amounts suitable for quantitation by GRIL-LC/MS. In addition to its use as an internal standard for quantitation, the A2G2' standard allowed us to determine which of the isobaric dp8 species was in fact A2G2' by it relative retention time and product ion profile. Thus, A2G2' is the only glycan metabolite that accumulates in disease that we have a complete structural determination for.

In total, 56 different glycan structures were detected in mouse brain and many of these were also detected in a number of different tissues and biological fluids taken from *GLB1* null mice showing that the enzymatic deficiency effects this class of substrate throughout the animal and not just in the CNS. The major differences we noticed involved the relative proportions of the various glycan metabolites and isoforms from tissue to tissue. For example, A2G2' levels were proportionately very low in brain and much higher in peripheral tissues and in urine. However, O-linked pentasaccharide levels were highest in the brain. All of the tissues as well as urine exhibited high levels of soluble glycans in affected mice. In contrast, plasma glycan metabolite levels were very low with only a few of the glycans seen in tissues and urine detected suggesting that these metabolites are cleared rapidly from the circulation.

While GRIL-LC/MS combined with data-dependent MS/MS to detect and structurally characterize soluble glycan metabolites is a more comprehensive approach for analyzing soluble glycans, it does have its limitations. It worked best with smaller more abundant oligosaccharides especially dp5 and dp6 isobars for which abundant product ions that include the aniline labeled reducing end are produced. Inter-ring cleavages resulting in neutral loss product ions gave insight into how the monosaccharide units that make up the parent species are arranged relative to the labeled reducing end. In addition, product ions formation was informative regarding what NRE residues are present. Thus it was possible to detect O-linked glycan metabolites and distinguish them from N-linked glycans. This approach, however, became less effective with larger oligosaccharides either because ion abundances were less for these larger species or because the only product ions observed were generated by the neutral loss of disaccharides and larger subunits. For example, the loss of a 365 Da subunit could be either a HexHexNAc or a HexNAcHex disaccharide. In the case of these larger species, we made no attempts to improve the quality of the data by injecting larger amounts or attempting to purify specific glycans since many were at lower relative abundance. For those isobaric species with higher abundances and more complete product ion formation, two structural signatures were important in determining oligosaccharide structure. The first was the existence of product ions with $m/z$ value consistent with a trihexose directly linked to aniline tagged HexNAc at the reducing end of the molecule. The reducing end product ion $Hex_2HexNAc$ is consistent with both the $Man_2GlcNAc$ core structure of N-linked glycans as well as a $Gal_2GalNAc$ sequence found in some O-linked glycans. The second important feature is the generation of two primary product ions, one generated by the neutral loss of a single Hex (presumably galactose) and the other generated by the loss of a single HexNAc. This profile is consistent with mucin type extended Core 1 and 2 O-linked glycans.

Mutations in the *GLB1* gene effecting β-galactosidase expression and activity lead to the development of two clinically distinct diseases. GM1 gangliosidosis, which is characterized by the accumulation of GM1, exhibits severe neurological symptoms. On the other hand, Morquio B (MPS IVB) results in the accumulation of keratan sulfate and is largely a skeletal disorder not associated with neuropathology [2,20,34]. In cases where GM1 gangliosidosis patients were tested, only modest increases in KS was detected compared to the very high levels seen in Morquio B patients. In addition, Morquio B patients don't appear to accumulate large amounts of gangliosides. Attempts to reconcile this paradox have centered on the notion that different sets of mutations within the *GLB1* gene can effect different sets of β-galactosidase substrates thus leading to the development of different clinical outcomes [34].

While same-patient human brain and urine samples were not available for this study, our results for urinary KS levels in human patients showed only modest increases in KS steady state levels in just a few of the patients tested. However, glycan metabolite levels as measured by A2G2', which appear to correlate well with ganglioside levels, where dramatically increased in all patients. Urinary KS levels were significant in age-matched normal controls and had levels at or higher than those detected in half of the affected patients. However, A2G2'

levels were below the limit of detection in all normal controls. These observations are consistent with the preferential-substrate model suggesting different types of *GLB1* mutations effecting distinct sets of substrates. Unfortunately, Morquio B patient samples were not available for this study so we were not able to determine if glycan metabolites increase in this lysosomal disorder as well or if they are specific for GM1 gangliosidosis. It will be interesting to analyze Morquio B patients for increases in glycan metabolites in order to better understand how different mutations can lead to different clinical outcomes and what factors contribute to those clinical fates.

The role played by oligosaccharide metabolites in GM1 gangliosidosis is not well understood but is likely to be significant. While we found more ganglioside accumulation in the *GLB1* null brain than the sum total of all soluble glycans, the accumulation of glycan metabolites in peripheral tissues, where ganglioside levels are normally low compared to the CNS, should be an important feature of this disease. Thus aspects of the disease outside of the CNS, such as hepatosplenomegaly and skeletal abnormalities, may be driven to some degree by glycans and not gangliosides. However, the accumulation of glycans in the CNS may be, along with ganglioside accumulation, also an important driver in the neuropathology of the disease. Consistent with this idea is the role played by soluble glycan accumulation in a related oligosaccharidosis disorder α-mannosidosis which is caused by a deficiency of α-mannosidase [38]. This disorder exhibits similar clinical symptoms to those of GM1 gangliosidosis including severe neurological deterioration. Interestingly, α-mannosidosis does not lead to the accumulation of gangliosides but instead only mannose-containing oligosaccharide metabolites which accumulate in the lysosomes of affected cells (see Fig. 1). Furthermore, since α-mannosidase deficiency effects predominantly N-linked glycans, the total amount of glycans accumulating in α-mannosidosis should be significantly lower than what is observed in GM1 gangliosidosis since the latter disease effects both N-linked and O-linked glycan metabolites both of which, we observed, show significant accumulation. The similar symptoms suffered by both GM1 gangliosidosis and α-mannosidosis patients suggests that the lysosomal accumulation of glycan metabolites can play an important role in the development of symptoms in both disorders and that gangliosides may not be the sole driver of pathology in GM1 gangliosidosis.

By monitoring different classes of accumulating GLB1 substrates, we are better equipped to evaluate multiple aspects of GM1 gangliosidosis. While many of the N-linked glycan metabolites we detected were observed in previous studies, our discovery of a number of N-glycan isobaric species as well as a number of new O-linked glycans adds a new dimension to our understanding of this disease. Importantly, we found that the steady state levels of these soluble glycan metabolites correlate well with those of gangliosides in this disease, potentially making them good surrogate biomarkers especially when considering their detection in an easily obtainable sample matrix such as urine. Measuring urinary levels of these glycans should make longitudinal studies and measuring the efficacy of new therapeutics much easier by eliminating the need for invasive analytical procedures. Furthermore, given the paucity of GM1 gangliosides in urine, urinary oligosaccharides such as A2G2' are attractive candidates for second tier biomarkers to confirm β-galactosidase activity measurements as part of newborn screening once successful therapies become available. Further work to validate these finding in a larger set of patients will be required to firmly establish the usefulness of measuring these metabolites for routine clinical analysis.

## 5. Conclusion

We carried out a comprehensive survey of β-galactosidase substrates that accumulate in a mouse model for GM1 gangliosidosis. These substrates include both gangliosides and soluble glycan metabolites which all have in common the definitive substrate for GLB1, β-linked galactose at their non-reducing ends. In addition to detecting N-glycan metabolites known to accumulate in this disorder, we discovered a number of species not previously described including species whose product ion spectra are consistent with metabolites derived from O-glycans. Many of these disease-related metabolites were also detected in affected human samples at significant levels. We developed a set of quantitative assays that assess multiple biomarkers impacted in this genetic disorder giving a more complete picture of disease severity and a larger panel of endpoints with which to evaluate the efficacy of new therapeutics.

## Acknowledgments

We gratefully acknowledge the NIH NeuroBioBank as the source of the human tissue. We thank the donors and their families for their invaluable donations for the advancement of science.

## Conflict of interest statement

RL, JVV, LM, SC, WC, AH, GY, JL and BEC are employees of and have interest in BioMarin Pharmaceutical Inc. NM is a former employee. RG and AD have collaborated with BioMarin Pharmaceutical Inc. during and outside of the conduct of this study.

## Appendix A. Supplementary data

Supplementary data to this article can be found online at https://doi.org/10.1016/j.ymgmr.2019.100524.

## References

[1] Regier, D. S., Tifft, C. J. (1993) GLB1-related disorders. GeneReviews((R)) (Adam, M. P., Ardinger, H. H., Pagon, R. A., Wallace, S. E., Bean, L. J. H., Stephens, K., Amemiya, A., Seattle (WA).
[2] C.R. Ferreira, W.A. Gahl, Lysosomal storage diseases, Transl. Sci. Rare Dis. 2 (2017) 1–71.
[3] G.C. Tsay, G. Dawson, Oligosaccharide storage in brains from patients with fucosidosis, GM1-gangliosidosis and GM2-gangliosidosis (Sandhoff's disease), J. Neurochem. 27 (1976) 733–740.
[4] E.W. Holmes, J.S. O'Brien, Hepatic storage of oligosaccharides and glycolipids in a cat affected with GM1 gangliosidosis, Biochem. J. 175 (1978) 945–953.
[5] T.G. Warner, J.S. O'Brien, Structure analysis of the major oligosaccharides accumulating in canine GM1 gangliosidosis liver, J. Biol. Chem. 257 (1982) 224–232.
[6] L.S. Wolfe, R.G. Senior, N.M. Ng-Ying-Kin, The structures of oligosaccharides accumulating in the liver of G-M1-gangliosidosis, type I, J. Biol. Chem. 249 (1974) 1828–1838.
[7] L. Bonesso, M. Piraud, C. Caruba, E. Van Obberghen, R. Mengual, C. Hinault, Fast urinary screening of oligosaccharidoses by MALDI-TOF/TOF mass spectrometry, Orphanet J. Rare Dis. 9 (2014) 19.
[8] C. Bruggink, B.J. Poorthuis, A.M. Deelder, M. Wuhrer, Analysis of urinary oligosaccharides in lysosomal storage disorders by capillary high-performance anion-exchange chromatography-mass spectrometry, Anal. Bioanal. Chem. 403 (2012) 1671–1683.
[9] P.R. Clements, Determination of sialylated and neutral oligosaccharides in urine by mass spectrometry, Curr. Protoc. Hum. Genet. (2012) 10 Chapter 17 Unit17.
[10] A. Klein, A. Lebreton, J. Lemoine, J.M. Perini, P. Roussel, J.C. Michalski, Identification of urinary oligosaccharides by matrix-assisted laser desorption ionization time-of-flight mass spectrometry, Clin. Chem. 44 (1998) 2422–2428.
[11] T. Ohkura, K. Yamashita, A. Kobata, Urinary oligosaccharides of GM1-gangliosidosis. Structures of oligosaccharides excreted in the urine of type 1 but not in the urine of type 2 patients, J. Biol. Chem. 256 (1981) 8485–8490.
[12] G.O. Peelen, J.G. de Jong, R.A. Wevers, HPLC analysis of oligosaccharides in urine from oligosaccharidosis patients, Clin. Chem. 40 (1994) 914–921.
[13] S.L. Ramsay, P.J. Meikle, J.J. Hopwood, P.R. Clements, Profiling oligosaccharidurias by electrospray tandem mass spectrometry: quantifying reducing oligosaccharides, Anal. Biochem. 345 (2005) 30–46.
[14] S. Tsuji, T. Ariga, S. Ando, Y. Tanaka, K. Kon, T. Yahagi, K. Ohta, T. Miyatake, Isolation and characterization of major urinary oligosaccharides excreted by a patient with type 3 GM1 gangliosidosis, J. Biochem. 109 (1991) 722–727.
[15] B. Xia, G. Asif, L. Arthur, M.A. Pervaiz, X. Li, R. Liu, R.D. Cummings, M. He, Oligosaccharide analysis in urine by maldi-tof mass spectrometry for the diagnosis of lysosomal storage diseases, Clin. Chem. 59 (2013) 1357–1368.
[16] K. Yamashita, T. Ohkura, S. Okada, H. Yabuuchi, A. Kobata, Urinary oligosaccharides of GM1-gangliosidosis. Different excretion patterns of oligosaccharides in the urine of type 1 and type 2 subgroups, J. Biol. Chem. 256 (1981) 4789–4798.
[17] M. Piraud, M. Pettazzoni, L. Menegaut, C. Caillaud, Y. Nadjar, C. Vianey-Saban, R. Froissart, Development of a new tandem mass spectrometry method for urine and amniotic fluid screening of oligosaccharidoses, Rapid Commun. Mass Spectrom. 31 (2017) 951–963.

[18] M. Casado, L. Altimira, R. Montero, E. Castejon, A. Nascimento, B. Perez-Duenas, A. Ormazabal, R. Artuch, A capillary electrophoresis procedure for the screening of oligosaccharidoses and related diseases, Anal. Bioanal. Chem. 406 (2014) 4337–4343.
[19] S.L. Ramsay, I. Maire, C. Bindloss, M. Fuller, P.D. Whitfield, M. Piraud, J.J. Hopwood, P.J. Meikle, Determination of oligosaccharides and glycolipids in amniotic fluid by electrospray ionisation tandem mass spectrometry: in utero indicators of lysosomal storage diseases, Mol. Genet. Metab. 83 (2004) 231–238.
[20] T. Okumiya, H. Sakuraba, R. Kase, T. Sugiura, Imbalanced substrate specificity of mutant beta-galactosidase in patients with Morquio B disease, Mol. Genet. Metab. 78 (2003) 51–58.
[21] R. Giugliani, M. Jackson, S.J. Skinner, C.M. Vimal, A.H. Fensom, N. Fahmy, A. Sjovall, P.F. Benson, Progressive mental regression in siblings with Morquio disease type B (mucopolysaccharidosis IV B), Clin. Genet. 32 (1987) 313–325.
[22] F.Q. Mayer, S. Pereira Fdos, A.H. Fensom, C. Slade, U. Matte, R. Giugliani, New GLB1 mutation in siblings with Morquio type B disease presenting with mental regression, Mol. Genet. Metab. 96 (2009) 148.
[23] R. Lawrence, S.K. Olson, R.E. Steele, L. Wang, R. Warrior, R.D. Cummings, J.D. Esko, Evolutionary differences in glycosaminoglycan fine structure detected by quantitative glycan reductive isotope labeling, J. Biol. Chem. 283 (2008) 33674–33684.
[24] B. Xia, C.L. Feasley, G.P. Sachdev, D.F. Smith, R.D. Cummings, Glycan reductive isotope labeling for quantitative glycomics, Anal. Biochem. 387 (2009) 162–170.
[25] C. Joseph, A.R.L. Chen, N. Wise, R. de Angelis, V. Agrawal, L. Mangini, J. Vincelette, B. Handyside, H. Sterling, M.J. Lo, H. Wong, N. Galicia, G. Pacheco, J. Van Vleet, A. Giaramita, S. Fong, M. Sushmita, C.H. Roy, R. Lawrence, S. Bullens, T.M. Christianson, A. d'Azzo, B.E. Crawford, S. Bunting, J.H. LeBowitz, G. Yogalingam, Intracerebroventricular enzyme replacement therapy with Beta-Galactosidase reverses brain pathologies due to GM1 gangliosidosis in mice, J. Biol. Chem. (2019) 1–35, https://doi.org/10.1074/jbc.RA119.009811 (Epub ahead of print, in press).
[26] R. Lawrence, H. Lu, R.D. Rosenberg, J.D. Esko, L. Zhang, Disaccharide structure code for the easy representation of constituent oligosaccharides from glycosaminoglycans, Nat. Methods 5 (2008) 291–292.
[27] C.N. Hahn, M. del Pilar Martin, M. Schroder, M.T. Vanier, Y. Hara, K. Suzuki, K. Suzuki, A. d'Azzo, Generalized CNS disease and massive GM1-ganglioside accumulation in mice defective in lysosomal acid beta-galactosidase, Hum. Mol. Genet. 6 (1997) 205–211.
[28] G.B. Mortuza, W.A. Neville, J. Delaney, C.J. Waterfield, P. Camilleri, Characterisation of a potential biomarker of phospholipidosis from amiodarone-treated rats, Biochim. Biophys. Acta 1631 (2003) 136–146.
[29] E.T. Baronas, J.W. Lee, C. Alden, F.Y. Hsieh, Biomarkers to monitor drug-induced phospholipidosis, Toxicol. Appl. Pharmacol. 218 (2007) 72–78.
[30] Z. Akgoc, M. Sena-Esteves, D.R. Martin, X. Han, A. d'Azzo, T.N. Seyfried, Bis (monoacylglycero)phosphate: a secondary storage lipid in the gangliosidoses, J. Lipid Res. 56 (2015) 1006–1013.
[31] R. Lawrence, J.R. Brown, K. Al-Mafraji, W.C. Lamanna, J.R. Beitel, G.J. Boons, J.D. Esko, B.E. Crawford, Disease-specific non-reducing end carbohydrate biomarkers for mucopolysaccharidoses, Nat. Chem. Biol. 8 (2012) 197–204.
[32] C. Baiotto, F. Sperb, U. Matte, C.D. da Silva, R. Sano, J.C. Coelho, R. Giugliani, Population analysis of the GLB1 gene in South Brazil, Genet. Mol. Biol. 34 (2011) 45–48.
[33] C.M. Silva, M.H. Severini, A. Sopelsa, J.C. Coelho, A. Zaha, A. d'Azzo, R. Giugliani, Six novel beta-galactosidase gene mutations in Brazilian patients with GM1-gangliosidosis, Hum. Mutat. 13 (1999) 401–409.
[34] J.W. Callahan, Molecular basis of GM1 gangliosidosis and Morquio disease, type B. structure-function studies of lysosomal beta-galactosidase and the non-lysosomal beta-galactosidase-like protein, Biochim. Biophys. Acta 1455 (1999) 85–103.
[35] D.A. Wenger, M. Sattler, W. Hiatt, Globoid cell leukodystrophy: deficiency of lactosyl ceramide beta-galactosidase, Proc. Natl. Acad. Sci. U. S. A. 71 (1974) 854–857.
[36] H. Tanaka, K. Suzuki, Lactosylceramide beta-galactosidase in human sphingolipidoses. Evidence for two genetically distinct enzymes, J. Biol. Chem. 250 (1975) 2324–2332.
[37] C. Bruggink, M. Wuhrer, C.A. Koeleman, V. Barreto, Y. Liu, C. Pohl, A. Ingendoh, C.H. Hokke, A.M. Deelder, Oligosaccharide analysis by capillary-scale high-pH anion-exchange chromatography with on-line ion-trap mass spectrometry, J. Chromatogr. B Anal. Technol. Biomed. Life Sci. 829 (2005) 136–143.
[38] Malm, D., and Nilssen, O. (1993) Alpha-Mannosidosis. in GeneReviews((R)) (Adam, M. P., Ardinger, H. H., Pagon, R. A., Wallace, S. E., Bean, L. J. H., Stephens, K., Amemiya, A., Seattle (WA).